Solitary waves in a granular chain of elastic spheres: Multiple solitary solutions and their stabilities

Zhi-Guo Liu,[1] Yue-Sheng Wang,[1,2,*] and Guoliang Huang[3]
[1]*Institute of Engineering Mechanics, Beijing Jiaotong University, Beijing 100044, China*
[2]*Department of Mechanics, School of Mechanical Engineering, Tianjin University, Tianjin 300350, China*
[3]*Department of Mechanical and Aerospace Engineering, University of Missouri, Columbia, Missouri 65211, USA*

(Received 30 December 2018; published 6 June 2019)

A granular chain of elastic spheres via Hertzian contact incorporates a classical nonlinear force model describing dynamical elastic solitary wave propagation. In this paper, the multiple solitary waves and their dynamic behaviors and stability in such a system are considered. An approximate KdV equation with the standard form is derived under the long-wavelength approximation and small deformation. The closed-form analytical single- and multiple-soliton solutions are obtained. The construction of the multiple-soliton solutions is analyzed by using the functional analysis. It is found that the multiple-soliton solution can be excited by the single-soliton solutions. This result is confirmed by the numerical analysis. Based on the soliton solutions of the KdV equation, the analytic solutions of multiple dark solitary waves are obtained from the original dynamic equation of the granular chain in the long-wavelength approximation. The stability of the single and multiple dark solitary wave solutions are numerically analyzed by using both split-step Fourier transform method and Runge-Kutta method. The results show that the single dark solitary wave solution is stable, and the multiple dark solitary waves are unstable.

DOI: 10.1103/PhysRevE.99.062904

I. INTRODUCTION

Propagation of acoustic and elastic waves in nonlinear phononic crystals has attracted great attention [1–5], because understanding of these dynamic behaviors not only offers the possibility of realizing nonlinear phenomena such as solitons [6–9] but also provides a powerful tool to manipulate the waves via nonlinearity [10–13].

Waves in linear [14,15] and nonlinear phononic crystals [16,17] exhibit quite different behaviors. For instance, waves cannot propagate freely through linear phononic crystals in the stop bands. But it was reported that different types of solitary waves, e.g., the KdV-like solitons [18–20], gap solitons [21–23], and gap breathers [24,25], can propagate in the stop bands through nonlinear phononic crystals. As is well known, a soliton is a solitary wave that can propagate stably with the dynamic behavior like a "particle." A solitary wave was shown to be an ideal method for transferring vibrational excitations [26]. Indeed, the discovery of phononic solitons has been demonstrated to be of fundamental importance in the study of nonlinear phenomena in phononic crystals. Recent results of nonlinear phononic crystals, such as sound bullets (a highly localized pulse) [27,28], novel granular protection systems [29], nonlinear phononic crystal waveguide [30], and highly nonlinear solitary waves [31], have shown potential applications of solitary waves in many fields.

In the present paper, we will discuss nonlinear phenomena related to elastic wave propagation in a nonlinear granular medium with periodical properties.

A granular medium chain of spheres is indeed a one-dimensional nonlinear phononic crystal. In periodically granular media, the dispersive effects are exhibited due to the reflection at the contact interface between two adjacent spheres. The nonlinear force between the spheres causes the waveform to converge and steep. Thus, the combination of dispersion and nonlinearity leads to the appearance of solitons [32]. Nonlinearly elastic wave propagation in granular crystals has received considerable attention in recent years (e.g., Refs. [33–43]). The dynamic behavior of nonlinear waves in granular media is very rich, e.g., traveling waves [44], shock waves [45], discrete breathers [24,46], nanoptera [47], and second solitary waves (SSWs) [48], etc. The system of a granular medium is tunable. It may be either weakly nonlinear in oscillatory regimes with high precompression or strongly nonlinear without precompression. This flexibility makes granular media useful in the areas of application such as energy trapping [49,50], energy harvesting [18], nonlinear waves sensor technology [51], acoustic lenses [28], acoustic diodes [52] and switches [53], and sound scramblers [54,55]. Although nonlinear solitary waves in granular chains have been studied extensively both experimentally and numerically [56], there are still many open problems, e.g. the existence and stability of solitary or multi-solitary wave solutions.

In Ref. [57], the numerical solitary wave solutions were obtained in an initially compressed chain of granular spheres. It was shown that the solutions have the same properties with the KdV equation's solutions. A KdV equation and its single-soliton solution were presented in Ref. [8] without detailed derivation. Two nonstandard KdV equations (Log-KdV equation and H-KdV equation) were obtained in a Fermi-Pasta-Ulam lattice with Hertzian-type potentials in Ref. [58].

*yswang@tju.edu.cn; yswang@bjtu.edu.cn

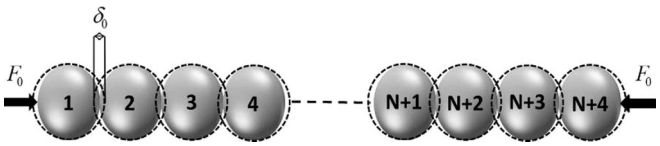

FIG. 1. Schematic diagram of the granular chain of elastic spheres precompressed by a static load.

The standard KdV equation was presented for the granular chains in the presence of precompression in Ref. [59].

In this paper, we consider the solitary waves propagating in a granular chain of spheres with precompression. A general standard KdV equation is derived based on the assumption of long-wavelength approximation and small deformation. It is obtained in the moving coordinate and slow-time scale and involves the parameters of the original system. The analytical single and multiple solitary solutions are obtained from the KdV equation by using the homogeneous equilibrium method [60–64] and Hirota's bilinear method [65]. The functional and numerical analysis of dynamic behaviors of the solutions are presented with emphasis on the relation between the multiple solitary waves and elastic collision between single solitary waves. Then, based on the dynamic analysis of the KdV equation's solutions, we construct the analytical single and multiple dark solitary solutions of the long-wavelength equation of the original granular chain. Finally, the stability of the solutions of the original system is discussed by using the Runge-Kutta and split-step Fourier transform method. The present research also provides further understanding of the chaotic behavior [66,67] and life-span [68] of solitary waves in chains of granular spheres.

II. MODEL AND DERIVATION OF KDV EQUATION

In this section, the model of a nonlinear wave propagation in a granular chain of elastic spheres with precompression will be established based on Ref. [57] and a KdV equation will be derived from the model. In the derivation, we assume the long-wavelength approximation and small deformation.

A. Model of a granular chain of spheres

Consider a granular chain of identical spheres with mass m precompressed by a staticload F_0; see Fig. 1, where δ_0 is the compression under the preset static load. According to the Hertzian contact theory [42], the relationship between F_0 and δ_0 is given by

$$F_0 = \frac{E(2R)^{1/2}}{3(1-\nu^2)}\delta_0^{3/2} = k_{\rm sph}\delta_0^{3/2}. \tag{1}$$

where R, ν, and E are the radius, Poisson's ratio, and Young's modulus of the spheres, respectively.

When a perturbed wave propagates through the chain, the spheres will vibrate with varying contact forces. Assume the central coordinate of the ith $(i = 1, 2, 3, \ldots)$ sphere is x_i. Then the relationship between the contact force, F, and compression, δ, between the ith and $(i+1)$th spheres is

$$F(\delta) = k_{\rm sph}\delta^{3/2} = k_{\rm sph}[2R - (x_{i+1} - x_i)]^{3/2}. \tag{2}$$

If the displacement of the ith sphere is denoted as y_i, then Newton's second law states

$$m\ddot{y}_i = F(\delta_0 - y_i + y_{i-1}) - F(\delta_0 - y_{i+1} + y_i). \tag{3}$$

The dynamic equilibrium condition, Eq. (3), combined with Eq. (2), can be transformed to

$$\ddot{y}_i = A(\delta_0 - y_i + y_{i-1})^{3/2} - A(\delta_0 - y_{i+1} + y_i)^{3/2}, \tag{4}$$

where

$$A = \frac{k_{\rm sph}}{m}, \tag{5}$$

is the Hertzian constant.

B. Derivation of KdV equation

Consider the situation that the static compression at the initial time is greater than the dynamic interparticle compression, i.e.,

$$\frac{|y_{i-1} - y_i|}{\delta_0} \ll 1.$$

Under this small dynamic deformation assumption, Eq. (4) reduces to (cf. Eq. (2.2) in Ref. [57])

$$\begin{aligned}\ddot{y}_i = {} & \tfrac{3}{2}A\delta_0^{1/2}(y_{i+1} - 2y_i + y_{i-1}) \\ & + \tfrac{3}{8}A\delta_0^{-1/2}(y_{i+1} - 2y_i + y_{i-1})(y_{i-1} - y_{i+1}),\end{aligned} \tag{6}$$

which, in the long-wavelength approximation, can be written in the continuous form:

$$\begin{aligned}y_{,tt} - c^2 y_{,xx} = {} & -\alpha c^2 y_{,x}y_{,xx} + \alpha\beta c^2 y_{,xxxx} \\ & - \frac{3\alpha^2\beta c^2}{10}y_{,xxxxxx} - 18\alpha^2\beta c^2 y_{,xx}y_{,xxx} \\ & - 9\alpha^2\beta c^2 y_{,x}y_{,xxxx},\end{aligned} \tag{7}$$

where $\alpha = R/\delta_0$; $\beta = R\delta_0/3$; and

$$c = \sqrt{6AR^2\delta_0^{1/2}} = \sqrt{6k_{\rm sph}m^{-1}R^2\delta_0^{1/2}}, \tag{8}$$

is the sound speed in the precompressed chain. Ignoring the infinitely small quantities of the fifth order, we obtain (cf. Eq. (2.3) in Ref. [57])

$$y_{,tt} = c^2 y_{,xx} + 2c\gamma y_{,xxxx} - \alpha c^2 y_{,x}y_{,xx}, \tag{9}$$

where $\gamma = \alpha\beta c/2$.

Assume that the solution of the above equation is of the form:

$$y(x,t) = f(\xi, T) + \epsilon y^{(1)}(x,t) + \epsilon^2 y^{(2)}(x,t) + \cdots, \tag{10}$$

where

$$\xi = x - ct, \quad T = \epsilon t, \tag{11a,b}$$

with ϵ being a small positive parameter. It is understood that ξ is a moving coordinate with speed c, and T is the slow time scale. Substituting Eq. (10) into Eq. (9) and ignoring all terms of order ϵ^2 and higher, we obtain

$$y^{(1)}_{,tt} - c^2 y^{(1)}_{,xx} = 2cf_{,\xi T} - c^2 f_{,\xi}f_{,\xi\xi} + c^2\beta f_{,\xi\xi\xi\xi}. \tag{12}$$

It is noted that f is a function of the moving coordinate ξ and slow-time T. Obviously, if the right side of Eq. (12) is

not equal to zero, then the solution $y^{(1)}$ will unlimitedly grow with the increasing of the quick-time t. So we can obtain from Eq. (12) a nonlinear wave equation:

$$2cf_{,\xi T} - c^2 f_{,\xi} f_{,\xi\xi} + c^2 \beta f_{,\xi\xi\xi\xi} = 0. \tag{13}$$

Introducing the transforms,

$$6u = f_{,\xi}, \quad \tau = \tfrac{1}{2}cT, \tag{14a,b}$$

we can finally transfer Eq. (13) into a KdV equation,

$$u_{,\tau} - 6uu_{,\xi} + \beta u_{,\xi\xi\xi} = 0, \tag{15}$$

where $\beta > 0$. It is noticed that the KdV Eq. (15) is obtained in the domain (ξ, T), which is a distorted mapping of the time-space domain (x, t). If we set $\beta = 1$ and $\tilde{u} = -u$, then Eq. (15) is the same as Eq. (8) in Ref. [59].

III. MULTIPLE-SOLITON SOLUTIONS OF KDV EQ. (15) AND THEIR DYNAMIC ANALYSIS

The multiple-soliton solutions of KdV Eq. (15) is well known. To study the dynamic behavior of the solitons based on the KdV equation, we will, for clarity and readability, directly present the exact single and multiple-soliton solutions of Eq. (15) in this section (the derivation using the homogeneous equilibrium method [60–64] and Hirota's bilinear method [65] is given in Appendix A). And then evolution and collision of the solitary waves will be analyzed. The analysis in this section is of particular importance to derive the solution of Eq. (9) in the next section.

The single-soliton solution is

$$u_1(\xi, \tau) = -2\beta \frac{k_1^2 e^{\theta_1}}{(1 + e^{\theta_1})^2}, \tag{16}$$

which can be rewritten as

$$u_1(\xi, \tau) = -\frac{1}{2}\beta k_1^2 \operatorname{sech}^2 \frac{k_1}{2}\left(\xi - \beta k_1^2 \tau\right), \tag{17}$$

where $\theta_1 = k_1\xi - \omega_1\tau$ with $\omega_1 = \beta k_1^3$; and k_1 is the wave number.

The double-soliton solution is

$$u_2(\xi, \tau) = -2\beta \frac{k_1^2 e^{\theta_1} + k_2^2 e^{\theta_2} + 2(k_1 - k_2)^2 e^{\theta_1+\theta_2}}{(1 + e^{\theta_1} + e^{\theta_2} + A_{12} e^{\theta_1+\theta_2})^2} - 2\beta \frac{A_{12}\left(k_2^2 e^{2\theta_1+\theta_2} + k_1^2 e^{\theta_1+2\theta_2}\right)}{(1 + e^{\theta_1} + e^{\theta_2} + A_{12} e^{\theta_1+\theta_2})^2}, \tag{18}$$

where $\theta_i = k_i\xi - \omega_i\tau$ with $\omega_i = \beta k_i^3$ $(i = 1, 2)$; k_i is the wave number; and $A_{12} = [(k_1 - k_2)/(k_1 + k_2)]^2$.

The triple-soliton solution is

$$u_3(\xi, \tau) = -2\beta \frac{\partial^2}{\partial \xi^2} \ln(1 + e^{\theta_1} + e^{\theta_2} + e^{\theta_3} + A_{12} e^{\theta_1+\theta_2} + A_{13} e^{\theta_1+\theta_3} + A_{23} e^{\theta_2+\theta_3} + A_{12}A_{13}A_{23} e^{\theta_1+\theta_2+\theta_3}), \tag{19}$$

where $\theta_i = k_i\xi - \omega_i\tau$ with $\omega_i = \beta k_i^3 (i = 1, 2, 3)$; k_i is the wave number; and $A_{ij} = [(k_i - k_j)/(k_i + k_j)]^2$ $(i, j = 1, 2, 3)$.

The quadruple-soliton solution is

$$u_4(\xi, \tau) = -2\beta \frac{\partial^2}{\partial \xi^2} \ln[\upsilon(\xi, \tau)], \tag{20}$$

where

$$\begin{aligned}\upsilon(\xi, \tau) = 1 &+ e^{\theta_1} + e^{\theta_2} + e^{\theta_3} + e^{\theta_4} + A_{12} e^{\theta_1+\theta_2} + A_{13} e^{\theta_1+\theta_3} \\ &+ A_{14} e^{\theta_1+\theta_4} + A_{23} e^{\theta_2+\theta_3} + A_{24} e^{\theta_2+\theta_4} + A_{34} e^{\theta_3+\theta_4} \\ &+ A_{12}A_{13}A_{23} e^{\theta_1+\theta_2+\theta_3} + A_{12}A_{14}A_{24} e^{\theta_1+\theta_2+\theta_4} \\ &+ A_{12}A_{14}A_{34} e^{\theta_1+\theta_3+\theta_4} + A_{23}A_{24}A_{34} e^{\theta_2+\theta_3+\theta_4} \\ &+ A_{12}A_{13}A_{14}A_{23}A_{24}A_{34} e^{\theta_1+\theta_2+\theta_3+\theta_4},\end{aligned}$$

with θ_i and A_{ij} being the same as in Eq. (19) with $i, j = 1, 2, 3, 4$.

It can be observed from Eq. (17) that the velocity (βk_1^2) is proportional to the amplitude. That is, the soliton travels in a granular chain of elastic spheres at the velocity depending on its amplitude; and the soliton with a high amplitude travels faster than the one with a low amplitude. Generally speaking, this conclusion is also true for other solitary waves traveling in a nonlinear and dispersive medium.

For the convenience of the dynamic analysis, the profiles of solitons Eqs. (17)–(20) are illustrated in Fig. 2 for some particular cases. It is seen that all solitons are highly localized. They are all bright solitary waves.

Figure 2(a) shows the profile of solution Eq. (17). Unlike an ordinary linear wave, a solitary wave is not periodic and is highly localized.

It is observed from the profile of the double-soliton Eq. (18) shown in Fig. 2(b) that the double-soliton looks like collision of two single-solitons, and they pass through each other without scattering but emerge from the collision having the same shape and velocity with which they entered. However, the double-soliton Eq. (18) of KdV Eq. (15) is not a superposition of two single-solitons. Since the KdV equation is nonlinear, the principle of superposition does not apply and so the sum of two single-solitons is not a solution of Eq. (15). Similarly, the triple- [Fig. 2(c)] or quadruple-soliton [Fig. 2(d)] looks like a collision of three or four single-solitons. The collision of the triple-soliton forms a small crest in the collision center, the peak of which is between two single-solitons; see Fig. 2(c). And the collision of the quadruple-soliton forms two small crests; see Fig. 2(d). It is obvious that the multiple-solitons are not superposition of the single-solitons.

A. Dynamic analysis of soliton solutions

The dynamic analysis of the interaction process of solitons is a very important topic in studies of nonlinear waves [7,26,32,67]. In the process of collision, the multiple-solitons may be excited. In this section, we will analyze the dynamic interaction process for the double-soliton solution Eq. (18) in details.

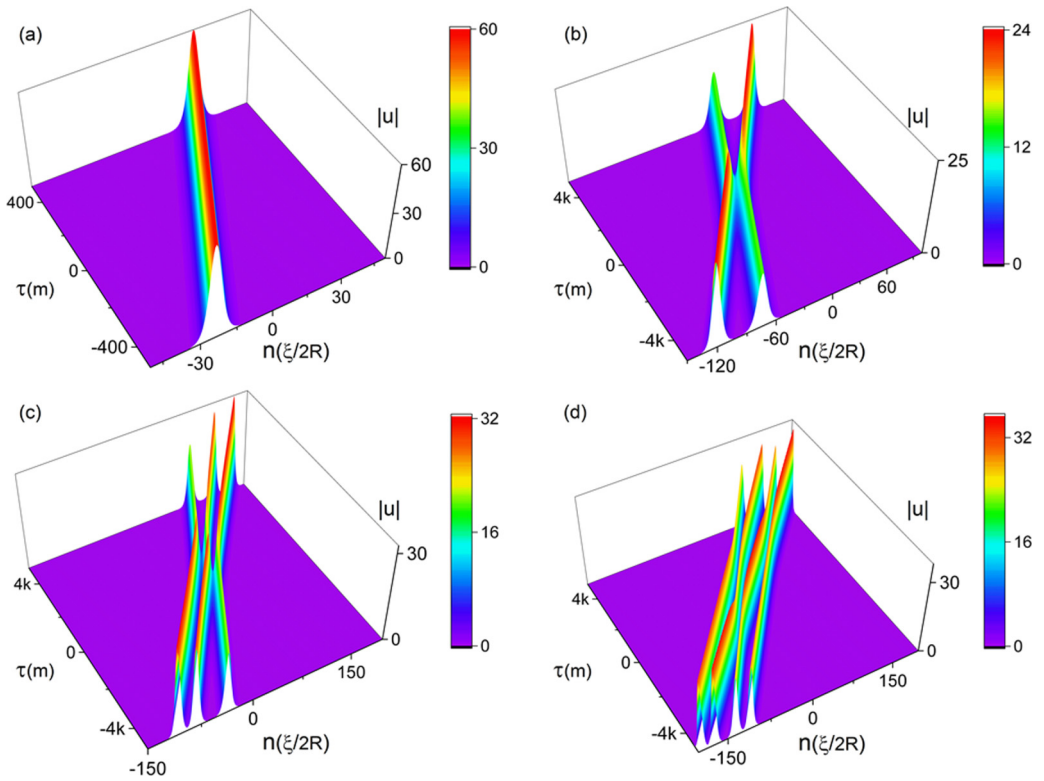

FIG. 2. The profiles of soliton solutions ($\beta = 1330\,\mu\text{m}^2$, $R = 2\,\text{mm}$): (a) solution Eq. (17) with $k_1 = 300\,\text{m}^{-1}$; (b) solution Eq. (18) with $k_1 = 150\,\text{m}^{-1}$ and $k_2 = -190\,\text{m}^{-1}$; (c) solution Eq. (19) with $k_1 = -180\,\text{m}^{-1}$, $k_2 = 220\,\text{m}^{-1}$, and $k_3 = 210\,\text{m}^{-1}$; and (d) solution Eq. (20) with $k_1 = 200\,\text{m}^{-1}$, $k_2 = 200\,\text{m}^{-1}$, $k_3 = -210\,\text{m}^{-1}$, and $k_4 = -230\,\text{m}^{-1}$.

1. Functional analysis

It is easy to find that $e^{\theta_i}(i = 1, 2)$ plays a major role in Eq. (18). In what follows, we will analyze the dynamic behavior of solution Eq. (18) in six different cases according to the range of e^{θ_i}.

Case (i): $e^{\theta_1} \approx 1$ and $e^{\theta_2} \ll 1$. In this case, we can remove e^{θ_2}-independent terms by setting $e^{\theta_2} \approx 0$. Then Eq. (18) becomes

$$u_2(\xi, \tau) \approx -2\beta k_1^2 \frac{e^{\theta_1}}{(1 + e^{\theta_1})^2}. \tag{21}$$

Case (ii): $e^{\theta_1} \approx 1$ and $e^{\theta_2} \gg 1$. Divide the numerator and denominator of the right-hand side of Eq. (18) by $e^{2\theta_2}$ and set $e^{-2\theta_2} \approx 0$. Then we have

$$\begin{aligned} u_2(\xi, \tau) &\approx -2\beta k_1^2 \frac{A_{12} e^{\theta_1}}{(1 + A_{12} e^{\theta_1})^2} \\ &= -2\beta k_1^2 \frac{e^{\theta_1 + \ln A_{12}}}{(1 + e^{\theta_1 + \ln A_{12}})^2} \\ &= -2\beta k_1^2 \frac{e^{k_1(\xi + k_1^{-1} \ln A_{12}) - \omega_1 \tau}}{(1 + e^{k_1(\xi + k_1^{-1} \ln A_{12}) - \omega_1 \tau})^2}. \end{aligned} \tag{22}$$

Case (iii): $e^{\theta_1} \ll 1$ and $e^{\theta_2} \approx 1$. In this case, we can remove e^{θ_1}-independent terms by setting $e^{\theta_1} \approx 0$. Then Eq. (18) becomes

$$u_2(\xi, \tau) \approx -2\beta k_2^2 \frac{e^{\theta_2}}{(1 + e^{\theta_2})^2}. \tag{23}$$

Case (iv): $e^{\theta_2} \approx 1$ and $e^{\theta_1} \gg 1$. Divide the numerator and denominator of the left-hand side of Eq. (18) by $e^{2\theta_1}$ and set $e^{-2\theta_1} \approx 0$. Then we have

$$\begin{aligned} u_2(\xi, \tau) &\approx -2\beta k_2^2 \frac{A_{12} e^{\theta_2}}{(1 + A_{12} e^{\theta_2})^2} \\ &= -2\beta k_2^2 \frac{e^{\theta_2 + \ln A_{12}}}{(1 + e^{\theta_2 + \ln A_{12}})^2} \\ &= -2\beta k_2^2 \frac{e^{k_2(\xi + k_2^{-1} \ln A_{12}) - \omega_2 \tau}}{(1 + e^{k_2(\xi + k_2^{-1} \ln A_{12}) - \omega_2 \tau})^2}. \end{aligned} \tag{24}$$

Figures 3(a)–3(e) illustrate the double-soliton solution Eq. (18) and approximate solutions Eqs. (21)–(24) with the highlighted areas corresponding to four limiting cases (i)–(iv). It is observed that the approximate solutions are in good agreement with the solution Eq. (18).

Because e^{θ_1}(or e^{θ_2}) plays a major role in the approximate solutions Eqs. (21) and (22) [or Eqs. (23) and (24)]. Therefore, we call them θ_1 (or θ_2) solitons.

From Fig. 3 we find that the double-soliton Eq. (18) looks like the elastic collision of two single θ_i solitons. The solitary waves Eqs. (21) and (22) and Eqs. (23) and (24) are the same except for the phase, which suggests that they are of the same expressions before and after the collision. That is, the solitons do not change in the amplitudes, but with the phase shifts after the collision. Next we will present detailed analysis for the phase shift of the θ_1 soliton.

It can be seen by comparing Eqs. (21) and (22) that the relative phase shift of the θ_1-solitary wave is $k_1^{-1} \ln A_{12} \overset{d.}{=} P_s$

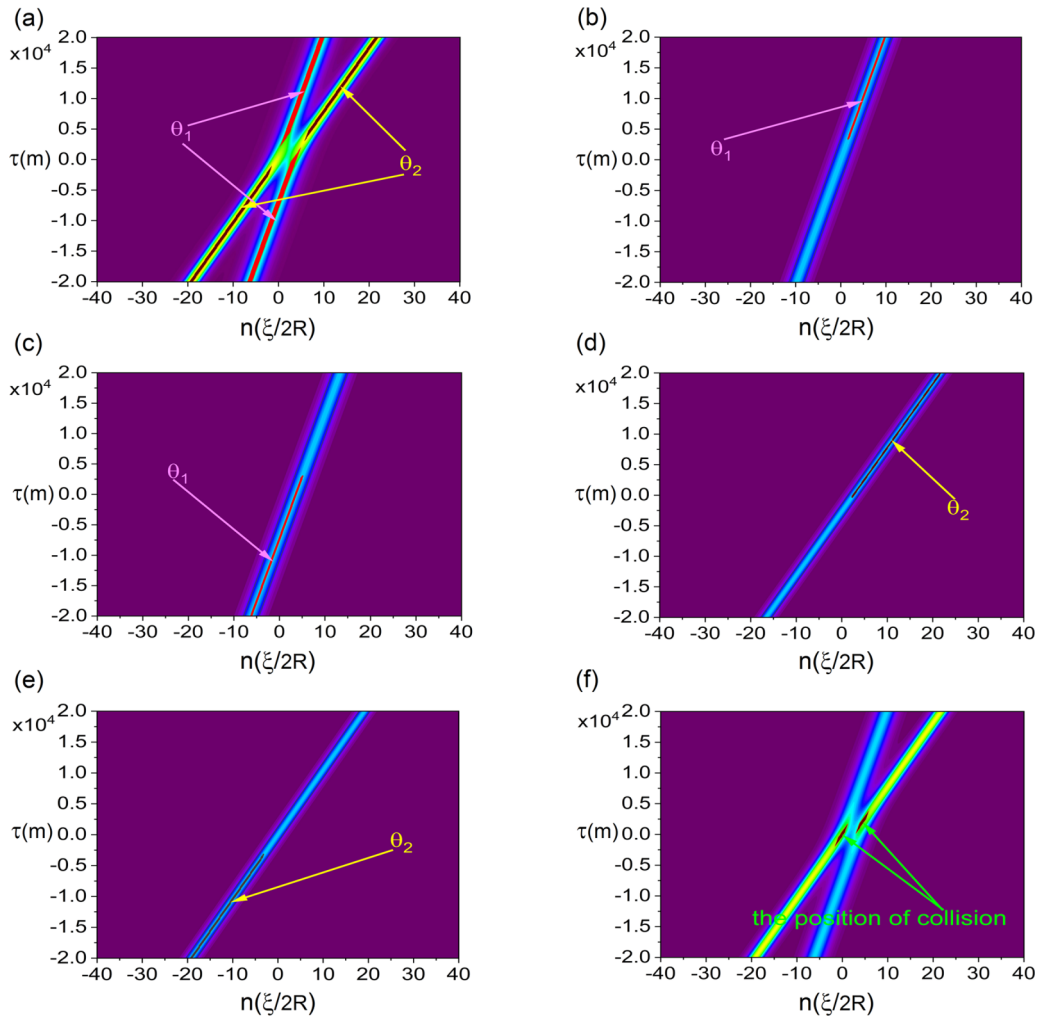

FIG. 3. Intensity profiles of the double-soliton solution Eq. (18) (a) and approximate solutions Eqs. (21)–(24) (b–e, respectively) with the highlighted areas corresponding to limiting cases (i)–(iv) where $\beta = 4887\,\mu\mathrm{m}^2$, $R = 2\,\mathrm{mm}$, $k_1 = 1\,\mathrm{m}^{-1}$, and $k_2 = 1.4\,\mathrm{m}^{-1}$.

after collision. For the particular example shown in Fig. 3, this value is $-3.5835\,\mathrm{m}$. Tracing the peak of the soliton from the numerical results, we can obtain the phase shift as $-3.5912\,\mathrm{m}$. The error between the theoretical and numerical values is less than 2%.

The phase shift is a distinguishing feature of the collision of solitons. It should be interesting to find the maximum phase shift. Recalling $A_{12} = [(k_1 - k_2)/(k_1 + k_2)]^2$, we know that $P_s = k_1^{-1} \ln A_{12}$ reaches positive or negative infinity when $k_2 = -k_1$. Without loss of generality, we set $k_1 = 1\,\mathrm{m}^{-1}$ and illustrate the phase shift P_s varying with k_2 in Fig. 4 (the other parameters are the same as described in the caption of Fig. 3). One can see that the phase shift becomes large as k_2 approaches $\pm k_1 (\pm 1)$. Figure 5(a) shows the double-soliton for $k_2 = 1.2\,\mathrm{m}^{-1}$. The phase shift of θ_1 soliton is $-4.7958\,\mathrm{m}$. It seems that the two solitons are traveling in almost parallel with a large phase transition.

The large phase transition may be used to regulate the solitons. We can perform the similar analysis and find the single θ_i solitons $(i = 1, 2 \cdots n)$ for the triple $(n = 3)$ or quadruple $(n = 4)$ soliton. After collision, θ_n soliton may be regulated by all other single θ_i solitons $(i < n)$. For instance, θ_2 solitons are regulated by θ_1 solitons as shown in Fig. 5(b) for the double-soliton; θ_3 solitons are regulated by θ_1 and θ_2 solitons as shown in Fig. 5(c) for the triple-soliton; and θ_4 solitons are regulated by θ_1, θ_2, and θ_3 solitons; see Fig. 5(d) for the quadruple-soliton. We observe that the phase shift of the θ_4 soliton is the biggest. We can use the phase change to

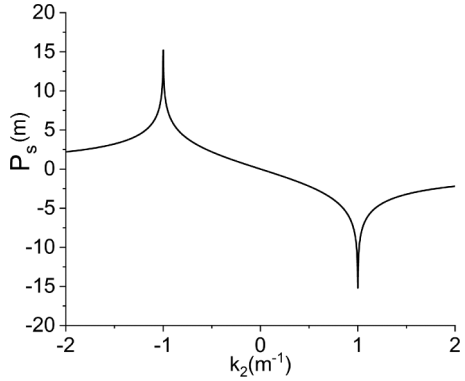

FIG. 4. Plot of the phase shift P_s for θ_1 soliton as the function of the wave number k_2. The other parameters are the same as described in the caption of Fig. 3.

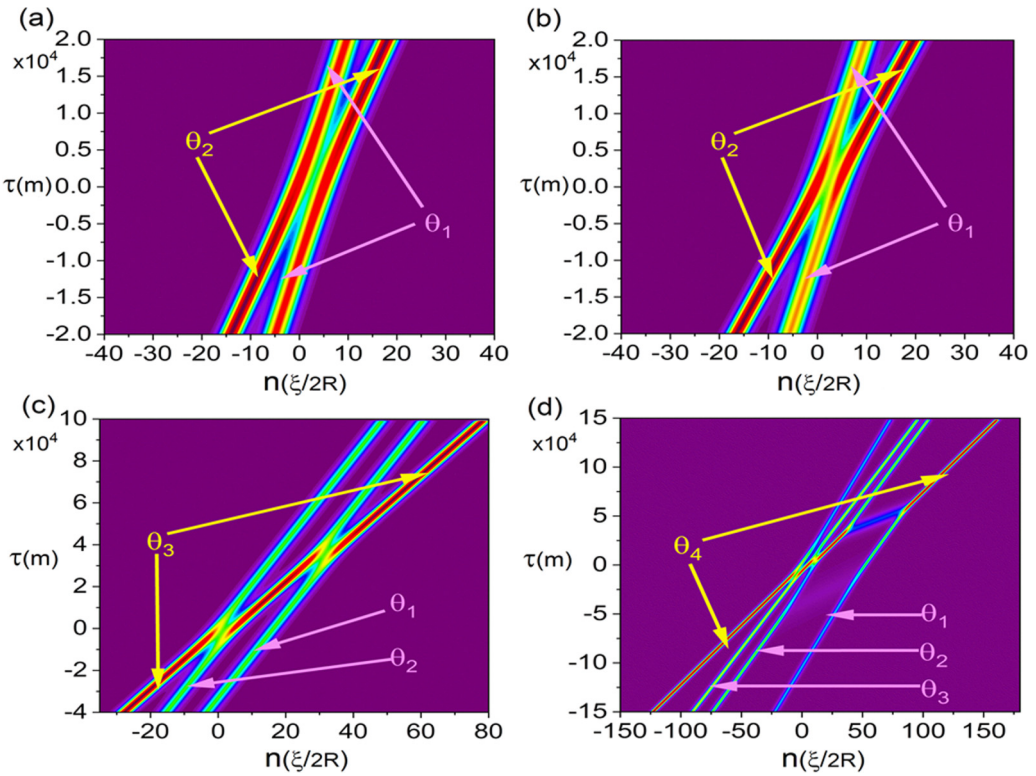

FIG. 5. Phase shifts of the $\theta_i (i = 1, 2, 3, 4)$-solitary waves: (a, b) intensity profiles of the double-soliton solution Eq. (18) with the areas marked with arrows showing θ_1- and θ_2-solitary waves for $k_1 = 1\,\mathrm{m}^{-1}$, $k_2 = 1.2\,\mathrm{m}^{-1}$ and $k_1 = 1\,\mathrm{m}^{-1}$, $k_2 = 1.3\,\mathrm{m}^{-1}$, respectively; (c) intensity profiles of the triple-soliton solution Eq. (19) with the area marked with arrows showing θ_1, θ_2, and θ_3 solitons for $k_1 = 1\,\mathrm{m}^{-1}$, $k_2 = 1.01\,\mathrm{m}^{-1}$, and $k_3 = 1.2\,\mathrm{m}^{-1}$; (d) intensity profiles of the quadruple soliton solution Eq. (20) with the area marked with arrows showing θ_1, θ_2, θ_3, and θ_4 solitons for $k_1 = 1\,\mathrm{m}^{-1}$, $k_2 = 1.1\,\mathrm{m}^{-1}$, $k_3 = 1.13\,\mathrm{m}^{-1}$, and $k_4 = 1.3\,\mathrm{m}^{-1}$. The other parameters are the same as described in the caption of Fig. 3.

accelerate (or decelerate) the soliton, e.g., the θ_4 soliton in Fig. 5(d) is accelerated.

Case (v): $e^{\theta_2} \approx 1$ and $e^{\theta_1} \approx 1$. In this case, we can get the following set of equations from Eq. (18):

$$k_1(\xi - \xi_1) - \omega_1\tau = 0,$$
$$k_2(\xi - \xi_2) - \omega_2\tau = 0,$$

which yields

$$\xi = \frac{\xi_1 k_2^2 - \xi_2 k_1^2}{k_2^2 - k_1^2}, \tau = \frac{\xi_2 - \xi_1}{\beta\left(k_1^2 - k_2^2\right)}. \tag{25}$$

Figure 3(f) shows the double-soliton solution Eq. (18) with the highlighted areas showing the position of the solitons before and after the collision in this special case, which can be obtained by tracing the peak of the soliton. However, the approximate analytical solution Eq. (25) yields the coordinates: $(\xi/2R, \tau) = (-2.663, -2545.6\,\mathrm{m})$ and (7.3163,2762.9 m). The approximate values and numerical results are identical with the difference smaller than 2%.

Case (vi): $e^{\theta_1} \gg 1$ ($e^{\theta_1} \ll 1$) and $e^{\theta_2} \gg 1$ ($e^{\theta_2} \ll 1$). This case includes four situations: (1) $e^{\theta_1}, e^{\theta_2} \gg 1$; (2) $e^{\theta_1}, e^{\theta_2} \ll 1$; (3) $e^{\theta_1} \gg 1$, $e^{\theta_2} \ll 1$; and (4) $e^{\theta_1} \ll 1$, $e^{\theta_2} \gg 1$. In all of these situations, the approximate solution of Eq. (15) is

$$u_2(\xi') \to 0. \tag{26}$$

The areas marked with dashed lines in Fig. 6 show the numerical results of the solution Eq. (18) under the conditions of $e^{\theta_1} \gg 1$ ($e^{\theta_1} \ll 1$) and $e^{\theta_2} \gg 1$ ($e^{\theta_2} \ll 1$). The marked areas are almost equal to zero. Also, the results of the analytical solution Eq. (26) are almost equal to zero with the same conditions as the solution Eq. (18) in these four limiting situations. So the approximate and numerical results are in good agreement.

The above analysis may be extended to the triple- or quadruple-solitons. Their dynamic behaviors are similar to those of the double-solitons. Therefore, to save space, we do not present here anymore.

In general, a multiple-soliton looks like elastic collision between single-solitons; and it may be represented approximately by the linear superposition of single-solitons in some limiting cases. This provides us a way to excite a multiple-soliton with the help of the single-solitons. It is known that if a stable solitary wave can still remain stable during the collisions, then such a solitary wave can be called a soliton. In published experimental and numerical investigations, the excitation of multiple-solitons was generally achieved through a single signal such as a Gaussian beam (or a single solitary wave) [69–71]. However, the input single signal does not necessarily converge to a single- or multiple-soliton after a certain evolution. It converges to a soliton only when there are some modes of stable solitary waves exist in the system. Therefore, the stability analysis of a solitary wave is very

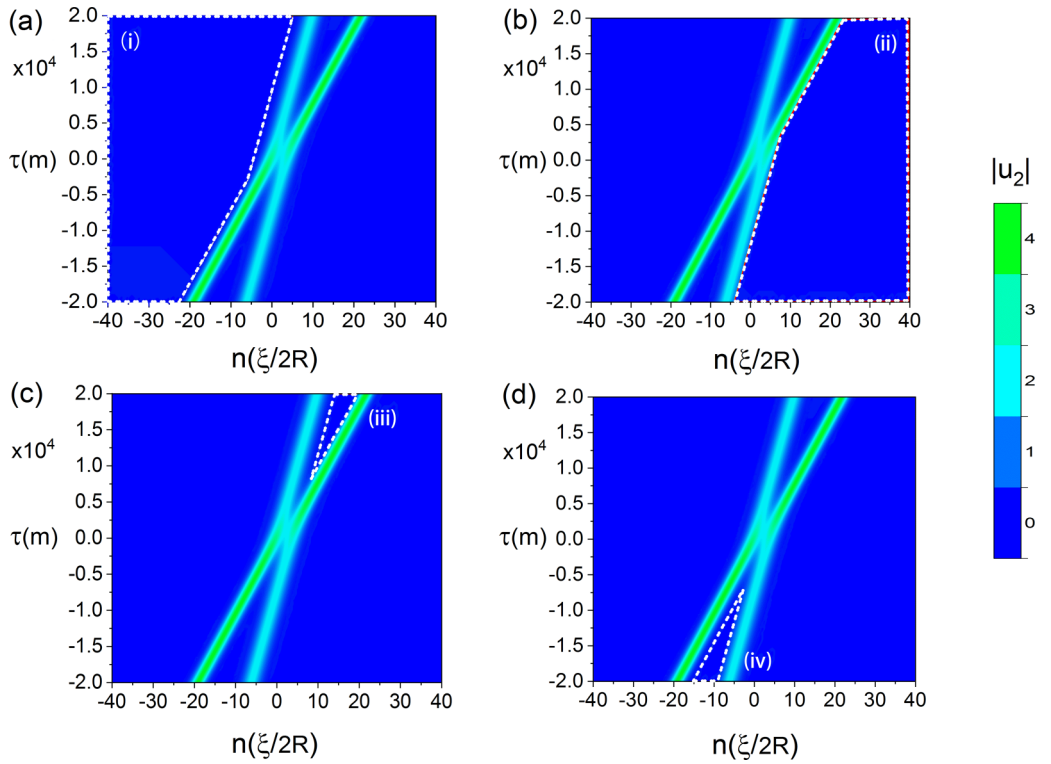

FIG. 6. The double soliton solution Eq. (18) shown by the areas marked with the dashed lines [(i), (ii), (iii), and (iv)] corresponding to four conditions: (a) $e^{\theta_1}, e^{\theta_2} \gg 1$; (b) $e^{\theta_1}, e^{\theta_2} \ll 1$; (c) $e^{\theta_1} \gg 1$, $e^{\theta_2} \ll 1$; (d) $e^{\theta_1} \ll 1$, $e^{\theta_2} \gg 1$. The parameters and the meaning of the highlighted areas are the same as described in the caption of Fig. 3.

important, and, of cause, is not a nontrivial task because the stability is related to many parameters of the system [63,64].

Next, we will present stability analysis of the solutions of KdV Eq. (15) using the split-step Fourier transform (SSFT) method [71].

2. *Numerical analysis*

SSFT method is a pseudospectral numerical method used to solve nonlinear partial differential equations. The method relies on computing the solution in small steps. It treats the dispersive and the nonlinear effects independently: first the nonlinearity step and then the dispersion step. Fourier transform is performed back and forth, because the dispersive step is made in the frequency domain while the nonlinear step is made in the time domain.

Next the SSFT method will be applied to solve Eq. (15) numerically to obtain a stable double solitary wave (i.e., a double-soliton). To this end, we use two methods to excite the double solitary wave. One method is to select the double-soliton solution Eq. (18) at $\tau = -5$ km with a perturbation of a random uniformly distributed noise field of amplitude 10^{-4} as the initial condition shown in Fig. 7(a). The other method is to select θ_1- and θ_2-soliton solutions Eqs. (22) and (24) with the same perturbation as the initial condition shown in Fig. 7(b). All the other parameters used are the same as in Fig. 3. The evolution results are shown in Figs. 7(c) and 7(d). It can be seen that both methods can excite the same stable double solitary waves. The two single solitary waves (i.e., θ_1 and θ_2 solitons) are remarkably stable, preserving their identities in the process of collision. This again confirms the conclusion in the last section that the double-soliton is inspired by elastic collision of two single-solitons.

Figure 8(a) shows the strong nonlinear interaction between two single-solitons during their collision. To understand the energy transferring in the collision process, we perform Fourier transform from the space-time domain [Fig. 8(a)] to the wave-number-frequency domain, see Fig. 8(b), which indeed gives the dispersion curve of the double-soliton solution. The responses in the time-wave-number domain and the space-frequency domain are presented in Figs. 8(c) and 8(d). It is seen from Fig. 8(c) that the intensity distribution of the spectrum is centered in the wave-number range from -4 to 4. The energy is continuously transferred from high to low wave numbers before the collision; then the inverse process appears after the collision. In Fig. 8(d), it is shown that the energy flows from high to low frequencies before the collision, and inversely after the collision. That is perhaps why we can inspire a stable double solitary wave (i.e., a double-soliton) using two single-solitons.

From Fig. 8, we can see that the collision of two single-solitons excites the double-soliton Eq. (18). It should be noticed that the collision of two single-solitons is the dynamic behavior of the single-soliton, but the double-soliton is the eigen-solution of the system. This is the distinguishing difference between a double-soliton and the collision of two single-solitons. Based on the above analysis, we can confirm that the existence of solitons is that the system has stable eigen-modes of double (or higher) solitary waves.

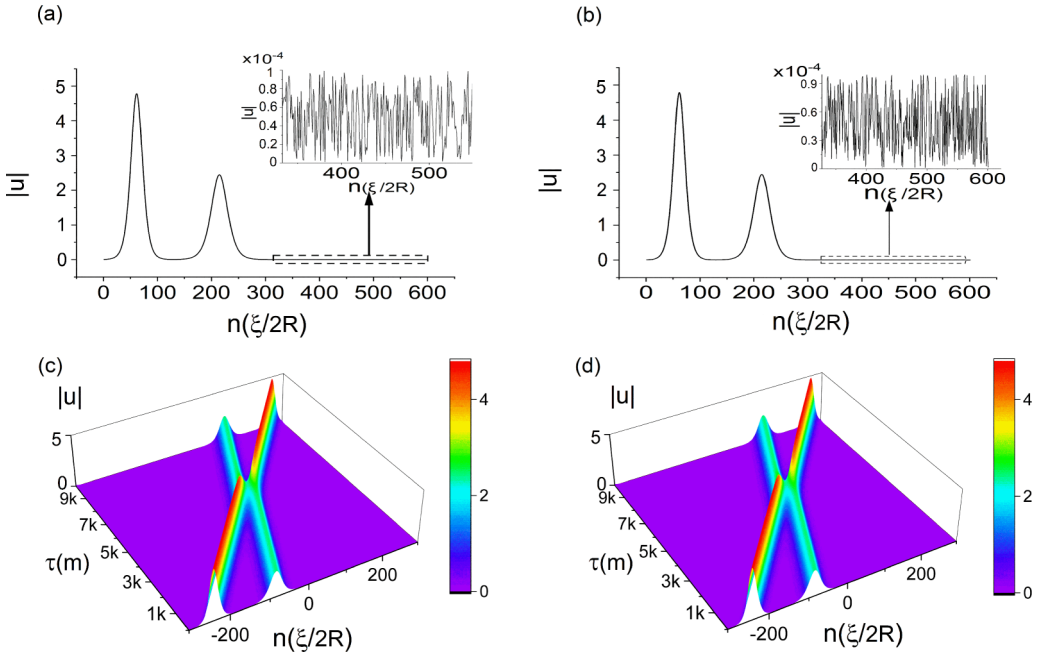

FIG. 7. Numerical simulation of a double-soliton inspired by a perturbed excitation with $\beta = 4887\,\mu\text{m}^2$, $R = 2\,\text{mm}$, $k_1 = 1\,\text{m}^{-1}$, and $k_2 = 1.4\,\text{m}^{-1}$: (a) initial condition selected from the double-soliton solution Eq. (18) with a perturbation; (b) initial condition selected from two single-soliton solutions Eqs. (21) and (24) with a perturbation; (c) evolution of the solution with the initial condition shown in (a); and (d) evolution of the solution with the initial condition shown in (b).

IV. ANALYTIC SOLITARY WAVE SOLUTIONS OF EQ. (9) AND THEIR STABILITY ANALYSIS

It is noted that Eq. (9) is obtained for a granular chain based on the assumption of long-wavelength approximation and small deformation without introducing any transformations such as distortion and rotation of the coordinate axes. That is to say, the solution of Eq. (9) can directly describe the dynamic behavior of the original system. However, the

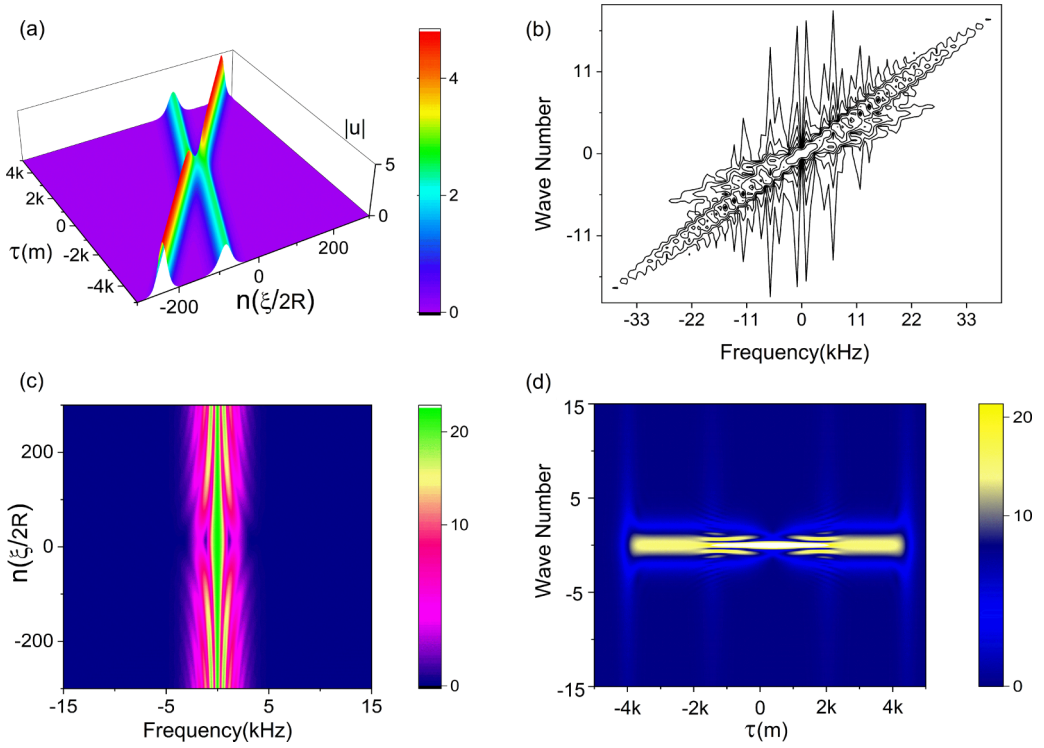

FIG. 8. Evolution of the double solitary wave solution Eq. (18) in the space-time domain (a) and wave-number-frequency domain (b). Panel (b) can also be viewed as the dispersion curve corresponding to panel (a); panels (c) and (d) show the energy transfer during the dynamic collision process in the time-wave-number domain and space-frequency domain, respectively.

KdV Eq. (15) is obtained from Eq. (9) through nonstandard coordinate transformations, Eqs. (11) and (14). That is, the solution of Eq. (15) may be viewed as a distorted mapping of the solution in the original system. So it is significant to find the solution of Eq. (9) for us to understand the dynamic behaviors of the solitary waves in the granular chain of elastic spheres.

It seems that the inverse transformations of Eqs. (11) and (14) can be used to derive the solutions of Eq. (9) from the solutions of Eq. (15) [i.e., Eqs. (16)–(20)]. However, the results may involve large errors. Next, an alternative method based on the above process will be used to obtain approximate solutions of Eq. (9). Especially, an exact single solitary solution is obtained fortunately.

A. Exact single solitary wave solution

From Eqs. (14a) and (16), we obtain

$$f_1(\xi,\tau) = 6\int u_1(\xi,\tau)\,d\xi = -6\beta k_1 \frac{e^{\theta_1}-1}{e^{\theta_1}+1} + C_1 + O(\epsilon^2)$$
$$= -6\beta k_1 \tanh\frac{\theta_1}{2} + C_1 + O(\epsilon^2), \tag{27}$$

where C_1 is an arbitrary constant and does not affect the basic behavior of f_1 (therefore we take $C_1 = 0$ to assure the symmetrical property of f_1 about $\xi = \tau = 0$). Equation (27), by using the inverse transformations of Eqs. (11) and (14b), yields the first term of Eq. (10), the approximate solution of Eq. (9). However, the solution may have a large error as mentioned above. To get a more precise solution, we suppose the solution has the form similar to Eq. (27),

$$y_1(x,t) = a_1 \tanh\frac{\overline{\theta}_1}{2}, \tag{28}$$

where $\overline{\theta}_1 = \overline{k}_1 x - \overline{\omega}_1 t = \overline{k}_1(x - \overline{c}_1 t)$ with $\overline{k}_1, \overline{\omega}_1$ (or $\overline{c}_1$) and a_1 to be determined. Substituting Eq. (28) into Eq. (9), and setting the coefficients of the same power exponents of $\tanh(\overline{\theta}_1/2)$ to be zero, we obtain

$$a_1 = -6\beta\overline{k}_1,\ \overline{\omega}_1 = \overline{k}_1\overline{c}_1, \tag{29a,b}$$

where

$$\overline{c}_1 = \pm\sqrt{6AR^2\delta_0^{1/2}\left(1+\frac{1}{3}\overline{k}_1^2R^2\right)}$$
$$= \pm c\sqrt{\left(1+\frac{1}{3}\overline{k}_1^2R^2\right)}$$
$$= \pm\sqrt{6k_{\rm sph}m^{-1}R^2\delta_0^{1/2}\left(1+\frac{1}{3}\overline{k}_1^2R^2\right)}, \tag{29c}$$

with c given by Eq. (8). Equation (29c) gives the speed of the single solitary wave which is bigger than the sound speed c. Finally, we obtain the exact single solitary wave solution of Eq. (9):

$$y_1(x,t) = -6\beta\overline{k}_1 \tanh\frac{\overline{\theta}_1}{2}. \tag{30}$$

The profiles of the displacement and its negative modulus $-|y_1|$ are displayed in Figs. 9(a) and 9(b), respectively. It is seen that the displacement solitary wave is a dark soliton. Its width is about five times of the spherical diameter, in accordance with the characteristic spatial size $10R$, which is clearly shown in Fig. 9(b). Although the solution [Eq. (27)] of KdV Eq. (15) and the solution [Eq. (30)] of Eq. (9) are of the same form, their dispersion relations are different; and the latter can give more accurate prediction to the solitary wave behavior than the former.

B. Approximate multiple solitary wave solutions

It is difficult to derive the exact multiple solitary wave solutions. However, in Sec. III A 2 we demonstrated that a multiple solitary wave can be viewed as the superposition of single solitary waves in some limiting situations. Therefore, the dispersion relation of a multiple solitary wave may be approximated by that of the single solitary wave [Eqs. (29b) and (29c)]. In addition, we compare Eqs. (27) and (30) and can find that these two equations have the same form with exchanging (ξ,τ,k_1,ω_1) with $(x,t,\overline{k}_1,\overline{\omega}_1)$. Based on this fact, we construct approximate multiple solitary wave solutions in the following way: integrate $u_i(\xi,\tau)(i=2,3,4)$ in Eqs. (18)–(20) w.r.t. ξ to obtain $f_i(\xi,\tau)$ from Eq. (14a); then replace (ξ,τ,k_1,ω_1) with $(x,t,\overline{k}_1,\overline{\omega}_1)$ to get the approximate solution for solitary waves. For the double solitary wave solution, we have

$$y_2(x,t) = 2a_2\frac{\overline{k}_1e^{\overline{\theta}_1} + \overline{k}_2e^{\overline{\theta}_2} + \overline{A}_{12}(\overline{k}_1+\overline{k}_2)e^{\overline{\theta}_1+\overline{\theta}_2}}{1+e^{\overline{\theta}_1}+e^{\overline{\theta}_2}+\overline{A}_{12}e^{\overline{\theta}_1+\overline{\theta}_2}}$$
$$+C_2 + O(\epsilon^2), \tag{31}$$

where C_2 is selected to satisfy the following condition:

$$\left|\int_{t_1}^{+\infty}\int_{x_1}^{+\infty}[y_2(x,t)-y_2(x_1,t_1)+C_2]dxdt\right| = \left|\int_{t_1}^{+\infty}\int_{-\infty}^{x_1}[y_2(x,t)-y_2(x_1,t_1)]dxdt\right|,$$
$$\left\{(x_1,t_1)|y_2(x_1,t_1) = \frac{\max[y_2(x,t_1)]+\min[y_2(x,t_1)]}{2}\right\}.$$

It will be extremely difficult to derive the expression of a_2 by directly inserting Eq. (31) into Eq. (9). Here we will follow the above limiting analysis in Sec. III A 1 to determine a_2. For instance, when $e^{\overline{\theta}_1} \approx 1$ and $e^{\overline{\theta}_2} \ll 1$, the solution Eq. (31) should reduce to single solitary wave solution Eq. (30), which yields $a_2 = -6\beta$. Similarly, we have

$$y_3(x,t) = -12\beta\frac{\overline{k}_1e^{\overline{\theta}_1}+\overline{k}_2e^{\overline{\theta}_2}+\overline{k}_3e^{\overline{\theta}_3}+\overline{A}_{12}(\overline{k}_1+\overline{k}_2)e^{\overline{\theta}_1+\overline{\theta}_2}+\overline{A}_{13}(\overline{k}_1+\overline{k}_3)e^{\overline{\theta}_1+\overline{\theta}_3}+\overline{A}_{23}(\overline{k}_2+\overline{k}_3)e^{\overline{\theta}_2+\overline{\theta}_3}}{1+e^{\overline{\theta}_1}+e^{\overline{\theta}_2}+e^{\overline{\theta}_3}+\overline{A}_{12}e^{\overline{\theta}_1+\overline{\theta}_2}+\overline{A}_{13}e^{\overline{\theta}_1+\overline{\theta}_3}+\overline{A}_{23}e^{\overline{\theta}_2+\overline{\theta}_3}+\overline{A}_{12}\overline{A}_{13}\overline{A}_{23}e^{\overline{\theta}_1+\overline{\theta}_2+\overline{\theta}_3}}$$
$$-12\beta\frac{\overline{A}_{12}\overline{A}_{13}\overline{A}_{23}(\overline{k}_1+\overline{k}_2+\overline{k}_3)e^{\overline{\theta}_1+\overline{\theta}_2+\overline{\theta}_3}}{1+e^{\overline{\theta}_1}+e^{\overline{\theta}_2}+e^{\overline{\theta}_3}+\overline{A}_{12}e^{\overline{\theta}_1+\overline{\theta}_2}+\overline{A}_{13}e^{\overline{\theta}_1+\overline{\theta}_3}+\overline{A}_{23}e^{\overline{\theta}_2+\overline{\theta}_3}+\overline{A}_{12}\overline{A}_{13}\overline{A}_{23}e^{\overline{\theta}_1+\overline{\theta}_2+\overline{\theta}_3}} + C_3 + O(\epsilon^2), \tag{32}$$

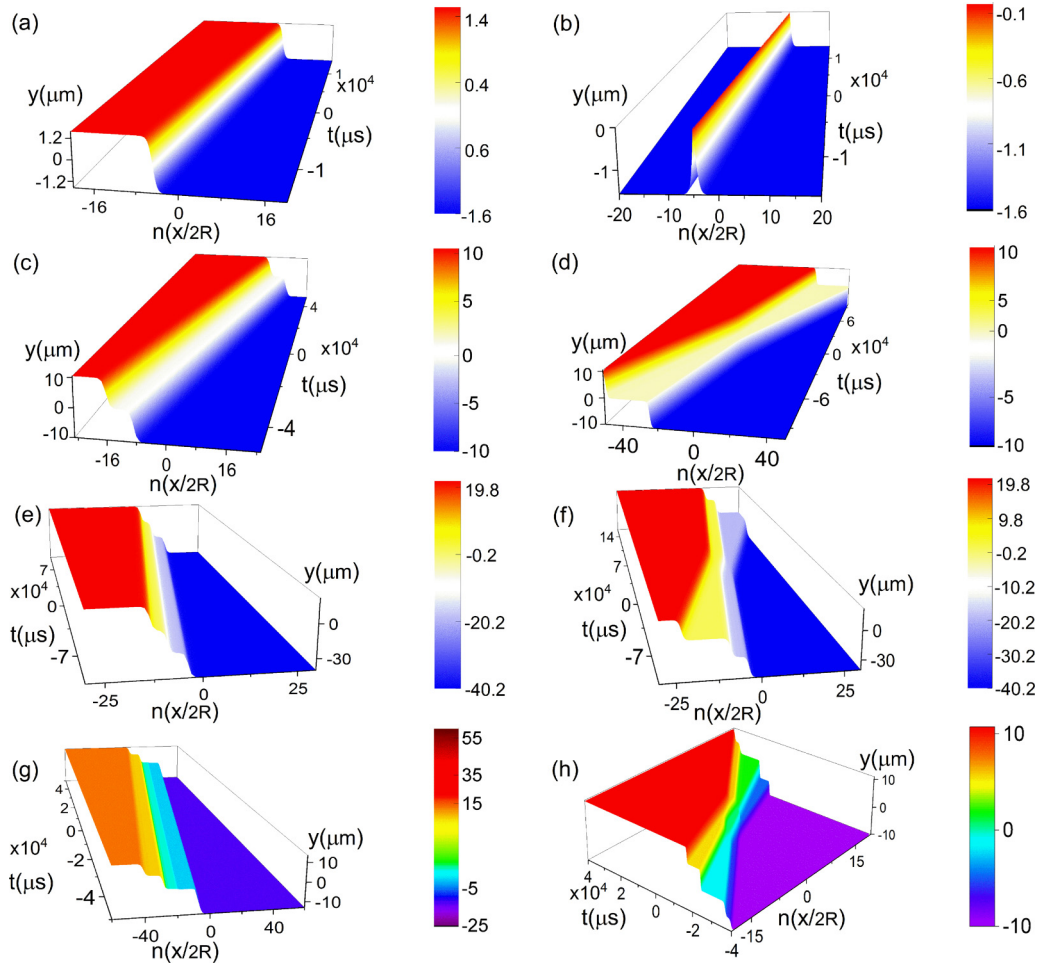

FIG. 9. The profiles of solitary wave solutions with the parameters listed in Table I: (a) solution Eq. (30); (b) negative modulus of solution Eq. (30); (c, d) solution Eq. (31); (e, f) solution Eq. (32); and (g, h) solution Eq. (33).

for the triple solitary wave solution, and

$$y_4(x,t) = -12\beta\left\{\int \frac{\partial^2}{\partial\xi^2}\ln[\nu(\xi,\tau)]d\xi\right\}_{(\xi,\tau,k_i,\omega_i)\to(x,t,\bar{k}_i,\bar{\omega}_i)} + C_4 + O(\epsilon^2), \tag{33}$$

for the quadruple solitary wave solution.

In Eqs. (31)–(33), $\bar{\theta}_i = \bar{k}_i x - \bar{\omega}_i t$, $\bar{\omega}_i = \pm\bar{k}_i\bar{c}_i$ and $\bar{A}_{ij} = [(\bar{k}_i - \bar{k}_j)/(\bar{k}_i + \bar{k}_j)]^2$. C_3 and C_4 are determined by the same condition as C_2. It can be proved that the above approximate solutions are of the second-order of ϵ (the proof is omitted here).

The displacement profiles of the double, triple and quadruple solitary waves, Eqs. (30)–(33), are shown in Figs. 9(a)–9(h). It is shown that all these displacement solitary waves are dark solitons and look like the collisions of single solitary waves especially when the velocities of the single solitary waves are quite different as shown in Figs. 9(d), 9(f) and 9(h). In Fig. 9(d) for the double solitary wave, the two single solitary waves keep their waveforms with significant phase changes after the collision; and their amplitudes are

TABLE I. The data used in Fig. 9.

Figure	$\beta\,(\mu m^2)$	$R\,(mm)$	$\bar{k}_1\,(m^{-1})$	$\bar{k}_2\,(m^{-1})$	$\bar{k}_3\,(m^{-1})$	$\bar{k}_4\,(m^{-1})$	$\bar{\omega}_1(s^{-1})$	$\bar{\omega}_2(s^{-1})$	$\bar{\omega}_3(s^{-1})$	$\bar{\omega}_4(s^{-1})$
(a), (b)	102.5	5	2.5500				20.4000			
(c)	416.7	5	2.0000	−2.1000			4.8870	−5.1313		
(d)	416.7	5	2.0000	−2.2100			4.8870	−10.2627		
(e)	814.5	5	2.0000	2.1000	−2.2000		2.0000	2.3100	−2.3047	
(f)	814.5	5	2.0000	2.1000	−2.2000		2.0000	4.6200	−2.3047	
(g)	416.7	5	1.2010	−1.2000	−1.5000	1.3980	5.8693	−5.8644	−7.3305	6.8320
(h)	55.6	5	8.0000	−6.0000	−10.0000	6.9900	78.1920	−29.3220	−74.2824	34.1601

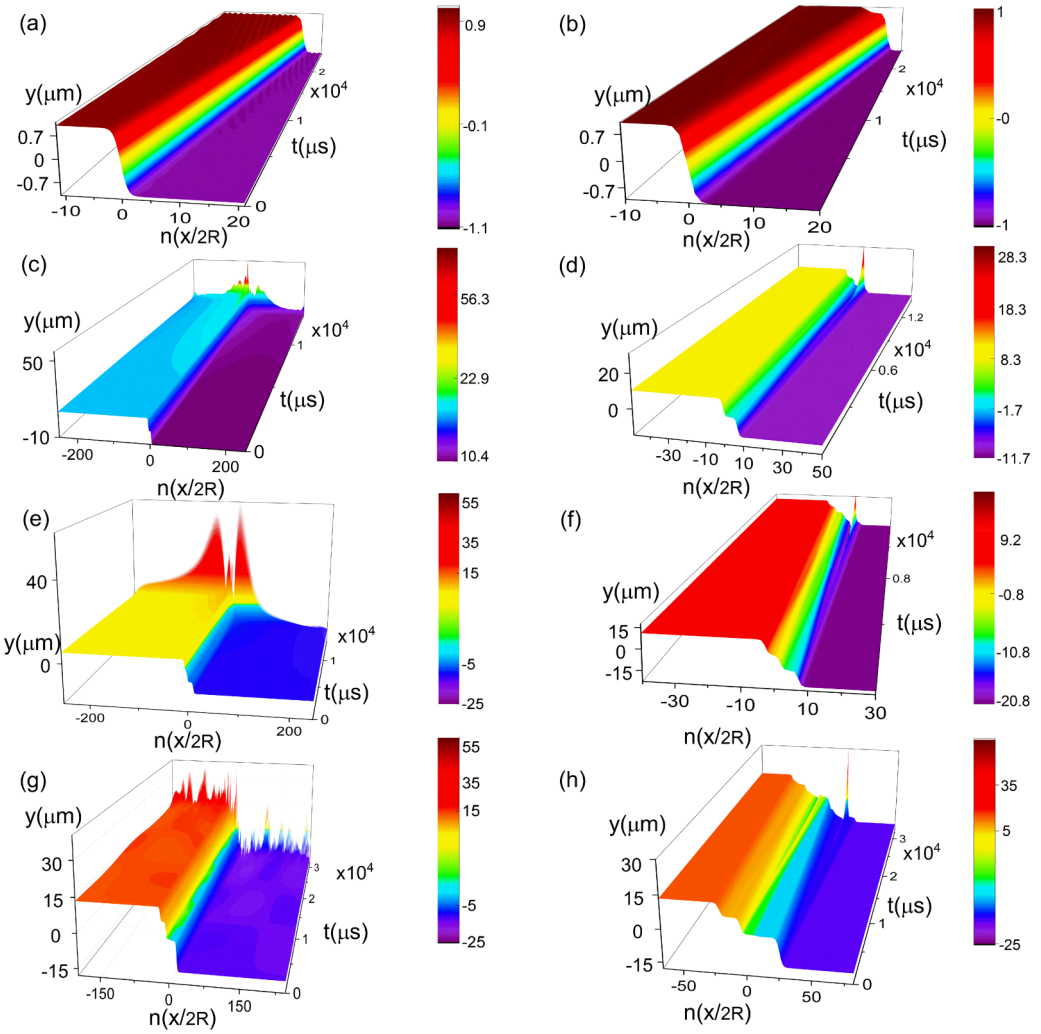

FIG. 10. Numerical simulation of the solitary waves inspired by a perturbed excitation at $t = 0$ with the parameters listed in Table II: (a), (c), (e), and (g) show evolution of the single, double, triple, quadruple dark solitary waves from Eq. (9) simulated by SSFT method; (b), (d), (f), and (h) show evolution of the single, double, triple, quadruple dark solitary waves from Eq. (6) simulated by Runge-Kutta method.

interchanged. For the triple solitary wave [Fig. 9(f)], all three single solitary waves keep their waveforms, but only the middle one changes its phase significantly; the other two interchange their amplitudes with slight phase changes. For the quadruple solitary wave [Fig. 9(h)], all four single solitary waves keep their waveforms and interchange their amplitudes; but no significant phase change is observed. Obviously, the collision does not satisfy the superposition principle as we mentioned before.

C. Stability analysis

Stability analysis of solitary waves is an important issue because only stable (or weakly unstable) solitary waves (self-trapped beams) can be observed in experiments [72].

In this section, we will first examine the stability of multiple solitary solutions obtained in the last section through two ways. One is to solve the long-wavelength approximate continuous Eq. (9) numerically using SSFT method; the other way is to solve the discrete Eq. (6) numerically using Runge-Kutta method [73]. Then we will perform numerical simulations of Eq. (4) which has no limitations of long-wavelength and small-dynamic compression. Stabilities analysis will be presented for all single and multiple solitary wave solutions, as well as a rogue wave solution.

1. Stability of dark solitary wave solutions of Eqs. (6) and (9)

We first examine the evolution stability of a single dark solitary solution by solving Eq. (9) numerically with SSFT method. To this end, we assume an initial excitation which is the displacement field from solution (30) at time $t = 0$ with a uniformly distributed random perturbation of amplitude 10^{-4} [63,73]. The evolution of the single dark solitary wave solution obtained from the Fourier transformation is demonstrated in Fig. 10(a) with $c = \sqrt{15}\,\mathrm{m/s}$, $\gamma = 0.01\,\mathrm{m^3/s}$, $\alpha = 1.3333 \times 10^6$ and other parameters listed in Table II. It is observed that the evolution of the solution is stable without losing its identity and integrity.

Then Runge-Kutta method is used to solve Eq. (6) to study the evolution of the single dark solitary wave solution. The result with the same parameters as in the SSFT method is

TABLE II. The data used in Fig. 10.

Figure	β (μm^2)	R (mm)	$\bar{k}_1$ (m^{-1})	$\bar{k}_2$ (m^{-1})	$\bar{k}_3$ (m^{-1})	$\bar{k}_4$ (m^{-1})	$\bar{\omega}_1$(s^{-1})	$\bar{\omega}_2$(s^{-1})	$\bar{\omega}_3$(s^{-1})	$\bar{\omega}_4$(s^{-1})
(a), (b)	166.70	63.2	1.0000				30.0000			
(c), (d)	416.65	10.0	2.0000	−2.1000			4.8870	−5.13135		
(e), (f)	416.65	10.0	1.0000	−1.1000	1.2000		2.4453	−2.6879	2.9322	
(g), (h)	416.65	33.3	1.2010	−1.2000	−1.5000	1.3980	5.8693	−5.8644	−7.3305	6.8320

shown in Fig. 10(b), which agrees well with the result by the SSFT method in Fig. 10(a). That is to say, both methods yield the same stable single dark solitary wave solution presented by Eq. (30).

Similar to the single solitary wave, a double dark solitary wave can be stimulated by the initial excitation of the perturbed displacement field from the analytical solution Eq. (31). Figures 10(c) and 10(d) illustrate the evolution of the double dark solitary wave simulated by both SSFT method [Fig. 10(c)] and Runge-Kutta method [Fig. 10(d)] for $c = \sqrt{2}\,\mathrm{m/s}$, $\gamma = 0.0012\,\mathrm{m^3/s}$, $\alpha = 1.6720 \times 10^6$ with other parameters listed in Table II. We can observe that the double solitary wave solution preserves its shape while propagating with a constant velocity at the early stage of the simulation. Later, however, the value of the solution increases exponentially, and the amplitude of the profiles spreads out in the chain. Clearly, the solution loses its identity and integrity, and no longer preserves the structure of a solitary wave solution. All these results suggest that the double dark solitary wave is unstable.

Similar numerical simulations of the evolution of the triple and quadruple dark solitary waves. The dark solitary wave solutions, Eqs. (32) and (33), are performed by using SSFT method and Runge-Kutta method. The results are shown in Figs. 10(e)–10(h) for $c = \sqrt{2}\,\mathrm{m/s}$, $\gamma = 0.0012\,\mathrm{m^3/s}$, $\alpha = 1.6720 \times 10^6$ with other parameters listed in Table II. These solitary waves are all unstable. They can only propagate stably with constant velocities in the early stage, and then become unstable in an exponential way.

2. *Stability of dark solitary wave solutions of Eq. (4)*

Unlike the discretization Eq. (6) and continuous Eq. (9), the discretization Eq. (4) is derived without assumption of long-wavelength and small dynamic deformation. Therefore, it would be interesting to check the stability of dark solitary waves by numerically simulating Eq. (4) that are initialized via perturbed solitary wave solutions of Eq. (9) or soliton solutions of KdV Eq. (15). It is noted that the initial excitations from the solutions of KdV Eq. (15) and the solutions of Eq. (9) are of the same form. For instance, at the initial moment $t = 0$, the displacement of the single solitary wave obtained from KdV Eq. (15) is given by Eq. (27), which has the same form as Eq. (30), the solution of Eq. (9). For the multiple solitary waves, we have the same conclusion. Therefore, simulations of Eq. (4) via the solutions of KdV Eq. (15) and the solutions of Eq. (9) yield the same results. Figure 11 presents evaluations of the single and multiple solitary waves

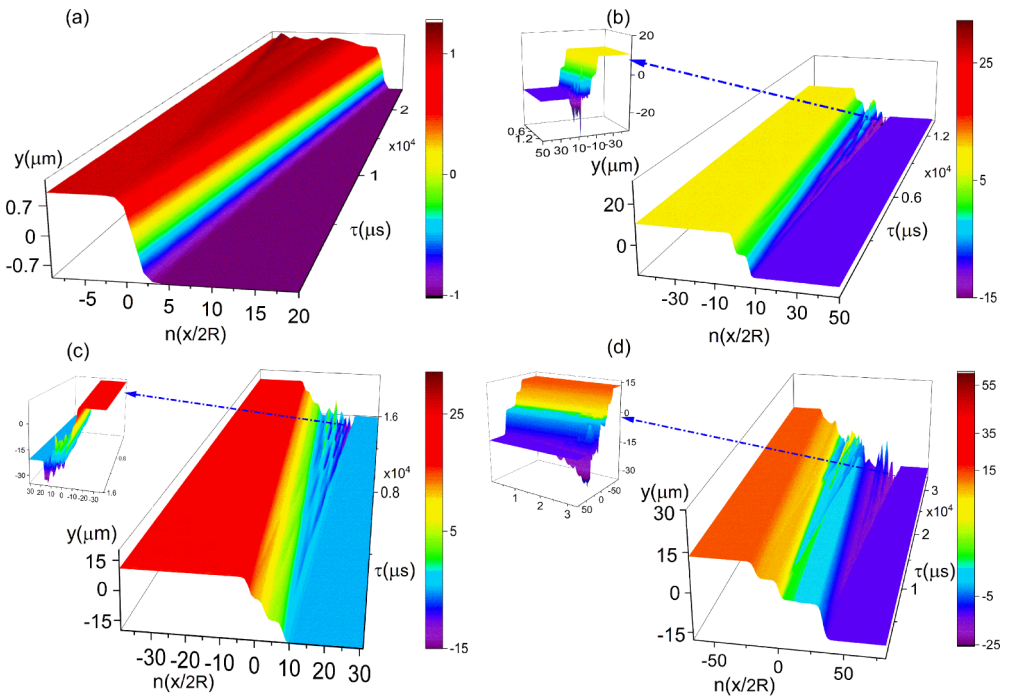

FIG. 11. Evolution of the single (a), double (b), triple (c), and quadruple (d) dark solitary waves simulated from Eq. (4) inspired by a perturbed excitation at $t = 0$ with the same parameters as in Fig. 10 by using Runge-Kutta method.

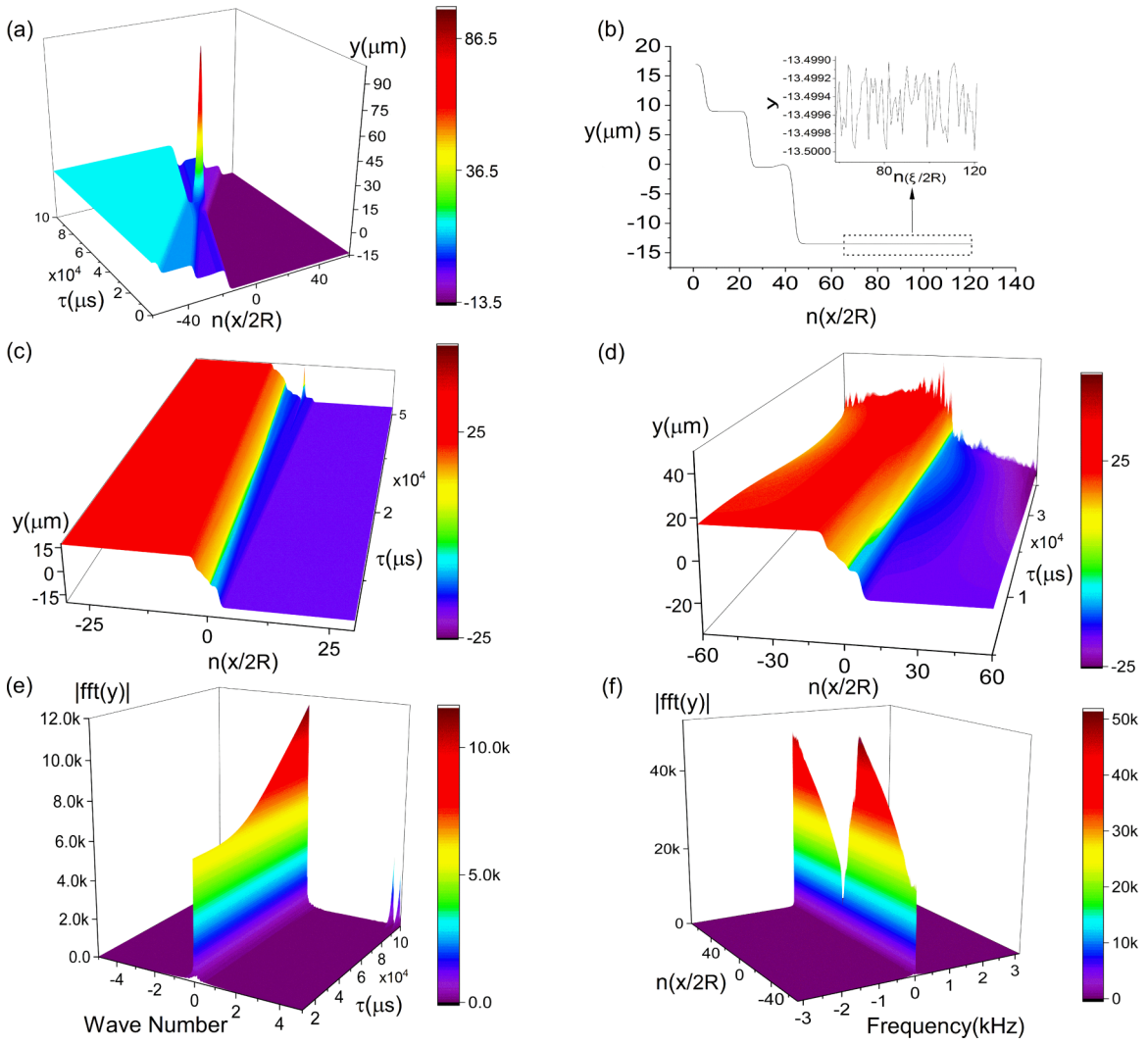

FIG. 12. (a) Evolution of the rogue wave obtained from Eq. (33) with $\beta = 416.65\,\mu\text{m}^2$, $R = 10.00\,\text{mm}$, $\overline{k}_1 = 1.6\,\text{m}^{-1}$, $\overline{k}_2 = -1.5\,\text{m}^{-1}$, $\overline{k}_3 = -1.9\,\text{m}^{-1}$, $\overline{k}_4 = 1.1\,\text{m}^{-1}$, $\overline{\omega}_1 = 15.6384\,\text{s}^{-1}$, $\overline{\omega}_2 = 7.3305\,\text{s}^{-1}$, $\overline{\omega}_3 = 14.1137\,\text{s}^{-1}$, and $\overline{\omega}_4 = 5.3757\,\text{s}^{-1}$; (b) initial condition selected from Eq. (33) at $t = 0$ with a perturbation; (c) evolution of the rogue wave from Eq. (6) simulated by Runge-Kutta method and corresponding to the initial conditions in panel (b); (d) evolution of the rogue wave from Eq. (9) simulated by SSFT method corresponding to the initial conditions; (e) solution in the time-wave-number domain, and (f) solution in the space-frequency domain corresponding to the evolution of the rogue wave in panel (d).

from Eq. (4) stimulated by Runge-Kutta method with the same parameters (including initial perturbation) as in Fig. 10. We can easily see from the figure that the single solitary wave is stable and the multiple solitary waves are unstable. These results are consistent with those from Eqs. (6) and (9) except that the perturbation growth rates in Fig. 11 are generally not as fast as those in Fig. 10. This, however, implies that Eqs. (6) and (9) satisfactorily describe the dynamic behavior of Eq. (4) under the long-wavelength limit and small dynamic compression assumption.

All simulations from Eqs. (4), (6), and (9) show that a dark single solitary wave can propagate stably in a strongly precompressed grannular chain of spheres ($|y_{i-1} - y_i| \ll \delta_0$). In fact, many authors have reported a stable single solitary wave propagating in a weakly precompressed chain ($\delta_0 \ll |y_{i-1} - y_i|$) (cf. Refs. [8,44]). It is noticed that Eq. (4) is valid for both strongly and weakly pre-compressed chain. If the solution Eq. (30) is used as an initial excitation to simulate Eq. (4) with $\delta_0 = 0$, then we can find a single solitary wave propagating stably in the system, meaning that Eq. (30) may be an approximate form of the solitary wave propagating in a weakly precompressed chain [44], see Appendix B for details.

Although the multiple dark solitary wave solutions in this paper are unstable, the degree of the instability of the multiple solitary wave solutions is different. Comparing the evaluation of the double solitary wave [Figs. 10(c), 10(d) and 11(b)] with those of the tripe [Figs. 10(e), 10(f) and 11(c)] and quadruple [Figs. 10(g), 10(h), and 11(d)] solitary waves, one can find that the double solitary wave maintain the characteristics of solitary waves well before the perturbation is sharply amplified, but the tripe and quadruple solitary waves cannot. Furthermore, the perturbations of tripe and quadruple solitary waves increase faster than that of the double solitary wave. Therefore, the double solitary wave is weakly unstable compared to the tripe and quadruple solitary waves.

It is known that errors may occur in the transmission computation. In this paper, the initial excitation is from the perturbed analytical solution; the error mainly comes from two aspects: (1) the length of the granular chain may affect the stability analysis when the solitary wave gets close to the end of the granular chain; and (2) with the increase of simulation time, the error of the program itself will accumulate gradually. Therefore, by controlling the magnitude of the errors generated from these two aspects within or less than the magnitude of the perturbation, the single dark solitary wave in this paper can be guaranteed to propagate steadily. We indeed did not find instability of the single dark solitary wave in our simulations based on Eqs. (4), (6), and (9).

3. A rogue wave solution and its stability

A rogue wave is a solitary wave with significant crest which appears in a highly localized area in the space-time domain, and then appears from nowhere and disappears without a trace [74,75]. Recently, Kevrekidis *et al.* [76] found that rogue waves may exist in the prototypical nonlinear mass-spring system and the diatomic granular crystal system. Similarly, rogue waves can also be found in the system studied in this paper. From the quadruple solitary wave solution Eq. (33), we indeed find a rogue wave as shown in Fig. 12(a). We select the quadruple solitary wave solution Eq. (33) at $t = 0$ with a perturbation of a random uniformly distributed noise field of amplitude 10^{-4} [see Fig. 12(b)] as the initial condition. Numerical simulations of the evolution of the quadruple solitary wave performed by using Runge-Kutta method and SSFT method are shown in Figs. 12(c) and 12(d), respectively. It is seen that the rogue wave is unstable.

Figures 12(e) and 12(f) present the solutions in the time-wave-number and space-frequency domains, respectively. In Fig. 12(e), only the spectrum near the central wave number increases obviously; and the spectra in other regions almost do not change. However, in Fig. 12(f) we find that the high-frequency spectrum remains almost unchanged, and the low-frequency spectrum increases dramatically. That is, the energy is transferred into the low-frequency region, causing a sharp increase of amplitude in a limited area in time domain. In conclusion, the exponential increase of the spectrum in the low-frequency region is also the cause of instability. Considering the instability of this solution, we can infer that there may be a singularity in the solution domain. This conclusion may be one of the reasons why rogue waves have strong destructiveness [77,78].

V. CONCLUSIONS

In this paper, the multiple solitary waves and their dynamic behaviors and stability in a granular chain of spheres are studied. The main results and conclusions may be summarized as follows:

(1) An approximate KdV equation is derived in the slow-time scale and moving coordinate from the dynamic equation of a granular chain of spheres under the long-wavelength approximation and small deformation. The closed-form analytical single and multiple (double, triple and quadruple) solitary wave solutions are obtained from the KdV equation.

(2) The detailed functional and numerical analysis of the single and multiple solitary waves in the KdV system are presented. It is shown that the single and double solitary waves are stable. The multiple solitary waves are the eigen-modes of the system other than the superposition of the single solitary waves. However, they can indeed be viewed as the linear superposition of single solitary waves in some limiting cases. This provides us a way to excite a multiple solitary wave using the single solitary waves.

(3) The exact analytic solution of a single dark solitary wave and approximate analytic solutions of multiple dark solitary waves are obtained from the original dynamic equation of the granular chain under the long-wavelength approximation and small deformation. Dynamic numerical analysis shows that single dark solitary wave is stable, while that the multiple dark solitary waves are unstable.

(4) The degree of the instability is different for different multiple solitary wave solutions. The double solitary wave is weakly unstable. The perturbations of triple and quadruple solitary waves increase faster than that of the double solitary wave.

(5) The unstable multiple dark solitary waves have different life-spans. Therefore, it should be an interesting topic to study the chaotic behavior and life-span of an unstable solitary waves in a granular chain of spheres.

(6) A rogue wave, which appears in a highly localized area in the space-time domain from nowhere and disappears without a trace, may exist in the granular chain.

ACKNOWLEDGMENTS

This work is supported by the Fundamental Research Funds for the Central Universities (Grant No. 2017YJS147), and National Natural Science Foundation of China (Grant No. 11532001).

APPENDIX A: SOLUTION TO KDV EQ. (15)

In this Appendix, we show the details of the derivation of the particular eignmode solutions to KdV Eq. (15). Based on the homogeneous equilibrium method, we assume that Eq. (15) has the following solution:

$$u(\xi,\tau) = -2\beta\frac{\partial^2}{\partial\xi^2}\ln g(\xi,\tau), \tag{A1}$$

which when substituted into Eq. (15) yields

$$(\ln g)_{,\xi\xi\tau} + 12\beta(\ln g)_{,\xi\xi}(\ln g)_{,\xi\xi\xi} + \beta(\ln g)_{,\xi\xi\xi\xi\xi} = 0, \tag{A2}$$

To reduce the calculation, we integrate Eq. (A2) over ξ once, let the integral constant be zero, and then have

$$(\ln g)_{,\xi\tau} + 6\beta(\ln g)^2_{,\xi\xi} + \beta(\ln g)_{,\xi\xi\xi\xi} = 0, \tag{A3}$$

Define the following bilinear operator [79]:

$$D_t^m D_x^n D_y^k D_z^l (g\cdot h) = \left(\frac{\partial}{\partial t} - \frac{\partial}{\partial t'}\right)^m \left(\frac{\partial}{\partial x} - \frac{\partial}{\partial x'}\right)^n \left(\frac{\partial}{\partial y} - \frac{\partial}{\partial y'}\right)^k \times \left(\frac{\partial}{\partial z} - \frac{\partial}{\partial z'}\right)^l (g\cdot h)\Big|_{x=x',y=y',z=z',t=t'}, \tag{A4}$$

where $g(x, y, z, t)$ and $h(x, y, z, t)$ are functions of x, y, x, t; and m, n, k, l are nonnegative integers. Then the following relations can be proved easily:

$$\begin{aligned}
D_t(g\cdot h) &= (g_{,t}h - gh_{,t'})\Big|_{t=t'} = g_{,t}h - gh_{,t},\\
D_t^2(g\cdot h) &= \Big(\frac{\partial}{\partial t} - \frac{\partial}{\partial t'}\Big)(g_{,t}h - gh_{,t})\Big|_{t=t'}\\
&= g_{,tt}h - 2g_{,t}h_{,t} + gh_{,tt},\\
D_t^3(g\cdot h) &= g_{,ttt}h - 3g_{,tt}h_{,t} + 3g_{,t}h_{,tt} + gh_{,ttt},\\
D_t^4(g\cdot h) &= g_{,tttt}h - 4g_{,ttt}h_{,t} + 6g_{,tt}h_{,tt} - 4g_{,t}h_{,ttt}\\
&\quad + gh_{,tttt},
\end{aligned} \tag{A5}$$

Considering the above properties of the bilinear operators, we obtain

$$\begin{aligned}
\frac{\partial^2 \ln g}{\partial\xi\,\partial\tau} &= \frac{1}{2g^2}[D_\xi D_\tau(gg)],\\
\frac{\partial^2 \ln g}{\partial\xi^2} &= \frac{1}{2g^2}\big[D_\xi^2(gg)\big],\\
\frac{\partial^4 \ln g}{\partial\xi^4} &= \frac{1}{2g^2}\big[D_\xi^4(gg)\big] - \frac{3}{2|g|^2}\big|D_\xi^2(gg)\big|^2.
\end{aligned} \tag{A6}$$

Substitution of Eq. (A6) into Eq. (A2) yields the Hirota bilinear form of Eq. (15):

$$\big(D_\tau D_\xi + \beta D_\xi^4\big)(gg) = 0, \tag{A7}$$

which can be solved by using Hirota's bilinear method. Expand g into a power series of a small parameter ϵ:

$$g(\xi,\tau) = \sum_{n=0}^{+\infty} g_n(\xi,\tau)\epsilon^n, \tag{A8}$$

which when substituted into Eq. (A7) yields

$$\sum_{n=0}^{+\infty}\epsilon^n\big(D_\tau D_\xi + \beta D_\xi^4\big)\Big(\sum_{m+l=n} g_m g_l\Big). \tag{A9}$$

Let the coefficient of each order of ϵ in Eq. (A9) be zero, we obtain

$$\big(D_\tau D_\xi + \beta D_\xi^4\big)\Big(\sum_{m+l=n} g_m g_l\Big) = 0, n \geqslant 0. \tag{A10}$$

For $n = 0, 1, 2, 3$, Eq. (A10) reduces to

$$\big(D_\tau D_\xi + \beta D_\xi^4\big)(g_0 g_0) = 0, \tag{A11}$$

$$\big(D_\tau D_\xi + \beta D_\xi^4\big)(g_1 g_0) = 0, \tag{A12}$$

$$2\big(D_\tau D_\xi + \beta D_\xi^4\big)(g_2 g_0) + \big(D_\tau D_\xi + \beta D_\xi^4\big)(g_1 g_1) = 0, \tag{A13}$$

$$2\big(D_\tau D_\xi + \beta D_\xi^4\big)(g_3 g_0) + 2\big(D_\tau D_\xi + \beta D_\xi^4\big)(g_2 g_1) = 0. \tag{A14}$$

Without of loss of generality, we set g_0 as a constant, and assume Eq. (A12) has an exponential eigen-solution:

$$g_1^j = e^{k_j\xi - \omega_j\tau + \delta_j}, \tag{A15}$$

which when substituted into Eq. (A12) yields

$$\big(\omega_j - \beta k_j^3\big)g_1^j g_0 = 0. \tag{A16}$$

Then we obtain the dispersion relation:

$$\omega_j - \beta k_j^3 = 0. \tag{A17}$$

The sum of the eigen-solution, Eq. (A15), w.r.t all or partial possible values of $j (j = 1 - N)$ also satisfies Eq. (A12). Therefore, we have the following eigen-solution:

$$g_1 = \sum_{j=1}^{N} g_1^j = \sum_{j=1}^{N} e^{\theta_j}, \theta_j = k_j x - \omega_j t + \delta_j, \tag{A18}$$

where k_j is the wave number; ω_j is the angular frequency; and δ_j is an arbitrary number.

Substitution of Eq. (A18) into Eq. (A13) yields

$$\begin{aligned}
&2\big(D_\tau D_\xi + \beta D_\xi^4\big)(g_2 g_0)\\
&= -\big(D_\tau D_\xi + \beta D_\xi^4\big)\Big(\sum_{i=1}^{N} e^{\theta_i}\sum_{j=1}^{N} e^{\theta_j}\Big)\\
&= \sum_{i=1}^{N}\sum_{j=1}^{N}[(\omega_i - \omega_j)(k_i - k_j) - \beta(k_i - k_j)^4]e^{\theta_i+\theta_j}\\
&= 2\sum_{1\leqslant i<j\leqslant N}[(\omega_i - \omega_j)(k_i - k_j) - \beta(k_i - k_j)^4]e^{\theta_i+\theta_j}.
\end{aligned} \tag{A19}$$

Considering the properties of the bilinear operators, we can obtain, from Eq. (A19),

$$g_2\cdot g_0 = \sum_{1\leqslant i<j\leqslant N} A_{ij}e^{\theta_i+\theta_j}, \tag{A20}$$

where

$$\begin{aligned}
A_{i,j} &= -\frac{(\omega_i - \omega_j)(k_i - k_j) - \beta(k_i - k_j)^4}{(\omega_i + \omega_j)(k_i + k_j) - \beta(k_i + k_j)^4}\\
&= \Big(\frac{k_i - k_j}{k_i + k_j}\Big)^2,
\end{aligned} \tag{A21}$$

where Eq. (A17) is considered.

Following the same process, we can obtain

$$g_3\cdot g_0 = -\sum_{\substack{1\leqslant i<j\leqslant N\\ 1\leqslant l\leqslant N}} A_{ij}e^{\theta_i+\theta_j+\theta_l}. \tag{A22}$$

All the other terms, $g_i (i = 4, \ldots, N)$, can be derived similarly. If we set $g_N = 0$ and $\epsilon = 0$, then we can obtain various eigen-solutions of Eq. (15). Next we present the single and double solitary wave solutions.

(i) The single solitary wave solution:

When $N = 1$, set $g_2 = 0$ and $g_0 = 1$. Then we have $g = 1 + g_1 = 1 + e^{\theta_1}$ with $\theta_1 = k_1\xi - \omega_1\tau (\delta_j = 0$ is assumed). Finally, we can obtain, from Eq. (A1), the single solitary wave solution, Eq. (16).

(ii) The double solitary wave solutions

When $N = 2$, set $g_3 = 0$ and $g_0 = 1$. Then we have $g = 1 + g_1 + g_2 = 1 + e_1^\theta + e_2^\theta + A_{12}e^{\theta_1+\theta_2}$ with $\theta_i = k_i\xi - \omega_i\tau$.

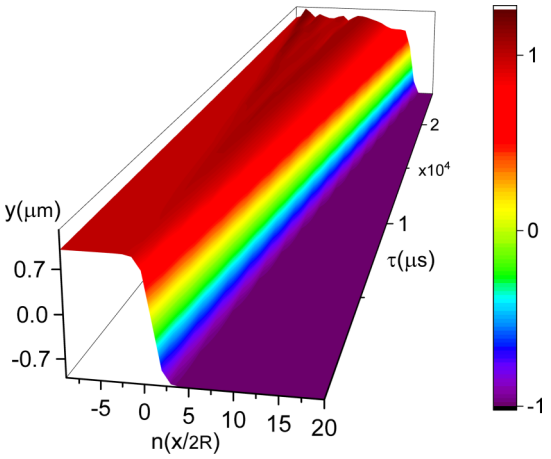

FIG. 13. Numerical simulation of the single solitary wave from Eq. (4) with $\delta_0 = 0$ inspired by a perturbed excitation at $t = 0$.

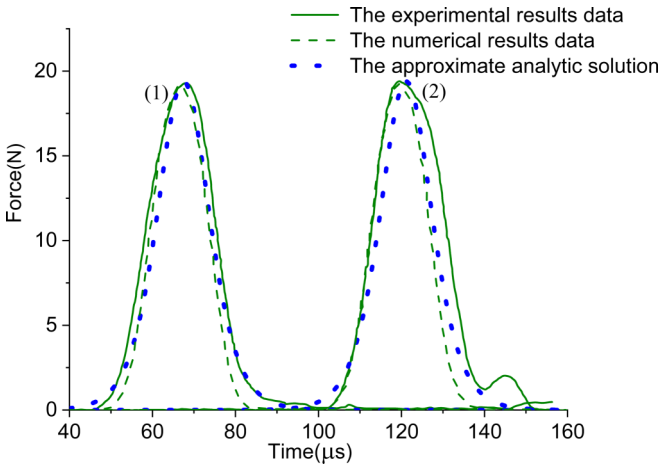

FIG. 14. Comparison between the present approximate analytical solutions with the experimental and numerical results in Fig. 3 of Ref. [80]: forces between the 7th and 13th particles in the chain of cylindrical particles with $\alpha = 90^\circ$.

Finally, we can obtain, from Eq. (A1), the double solitary wave solution, Eq. (18).
The other multiple (triple, quadruple,...) solitary solutions of Eq. (15) can be obtained similarly.

APPENDIX B: A STABLE SINGLE SOLITARY WAVE IN A WEAKLY COMPRESSED CHAIN OF GRANULAR

Although the present paper focuses on the precompressed granular chain, here in this Appendix we are interested in the case of $\delta_0 \to 0$ [57]. To this end, we use the single solitary wave solution Eq. (30), although it is for the precompressed chain, as the initial condition to study the dynamic behavior of Eq. (4) with $\delta_0 = 0$. Select the same parameters (including perturbation) as in Fig. 11(a). The numerical simulation from Eq. (4) with $\delta_0 = 0$ is illustrated in Fig. 13. We can see a single solitary wave propagating stably.

A stable single solitary wave propagating in the weakly precompressed chain has been observed experimentally in many literatures, e.g., Ref. [80] where a vertical chain consisting of 20 stainless steel cylindrical particles was considered. When the orientation angle (α) between the axes of two adjacent cylinders is 90°, the relation between the contact force $F_{\rm cy}$ and the compression δ can be obtained as in Ref. [80]:

$$F_{\rm cy}(\delta) = \frac{2E\sqrt{R}}{3(1-\nu^2)}\delta^{3/2} = k_{\rm cy}\delta^{3/2}, \tag{B1}$$

which is exactly of the same form as Eq. (1) for spheres. That is to say, the cylindrical particles chain for the case of $\alpha = 90^\circ$ [80] is equivalent to the spheres chain in the present paper. In Ref. [80], the chain was impacted to excite a single pulse, and the forces in the central plane of the 7th and 13th cylindrical particles were measured by using the piezoelectric sensors. The numerical simulation based on the finite element method was also performed. Both experimental (solid curves) and numerical (dashed curves) results from [80] are re-plotted in Fig. 14. Here we will show that the solution with the form of Eq. (30) is comparable to the results of Ref. [80]. Notice that Eq. (30) is an eigen-solution. Therefore, to match the initial excitation, we introduce an amplitude adaptor A_0 and a phase adaptor ζ. Then we suppose a solitary solution with the form of Eq. (30):

$$y(x_i, t) = -2A_0 R \tanh\left[\frac{\bar{k}_1}{2}(x_i - \bar{c}_1 t) + \zeta_0\right]. \tag{B2}$$

Under the assumption of continuum, the granular chain may be approximated to a solid bar of which the perturbed dynamic inner force may be approximately obtained by taking the first derivative of position of the relation Eq. (B2) and multiply it by the Young's modulus E and an effective contact area S_e:

$$\begin{aligned} F(x_i, t) &= ES_e\frac{\mathrm{d}y}{\mathrm{d}x} \\ &= EA_0S_eR\bar{k}_1\,\mathrm{sech}^2\left[\frac{\bar{k}_1}{2}(x_i - \bar{c}_1 t) + \zeta_0\right]. \end{aligned} \tag{B3}$$

According to Ref. [80], we have the Poisson's ratio $\nu = 0.3$, Young's modulus $E = 1.93 \times 10^{11}\,\mathrm{N/m^2}$, the cylindrical particle mass $m = 0.68 \times 10^{-3}\,\mathrm{kg}$; the radius $R = 2.38 \times 10^{-3}\,\mathrm{m}$. Select $A_0S_e = 9.583 \times 10^{-9}\,\mathrm{m^2}$, $\bar{k}_1 = 442\,\mathrm{m^{-1}}$, $\bar{c}_1 = 540.4\,\mathrm{m/s}$ and $\zeta_0 = 1.1625$. Then Eq. (B3) becomes

$$F(x_i, t) = 19.456\,\mathrm{sech}^2[221(x_i - 540.4t) + 1.1625], \tag{B4}$$

where the SI system is applied.

Figure 14 illustrates the forces between the 7th and 13th particles from Eq. (B4), together with the experimental and numerical results in [80]. It is shown that the analytical solution Eq. (B4) is in accordance with the results in Ref. [80].

[1] S. Rudykh and M. C. Boyce, Phys. Rev. Lett. **112**, 034301 (2014).
[2] X. Fang, J. Wen, J. Yin, D. Yu, and Y. Xiao, Phys. Rev. E **94**, 052206 (2016).
[3] Y. Yun, G. Q. Miao, P. Zhang, K. Huang, and R. J. Wei, Phys. Lett. A **343**, 351 (2005).
[4] R. J. Leveque, SIAM J. Appl. Math. **63**, 1539 (2003).
[5] D. I. Ketcheson and M. Q. de Luna, J. Sci. Comput. **58**, 672 (2014).
[6] E. Fermi, J. Pasta, and S. Ulam, *Studies of Nonlinear Problems. Collected Papers*, Vol. II (University of Chicago Press, 1955), pp. 977–988.
[7] M. F. Hamilton and D. T. Blackstock, *Nonlinear Acoustics* (Academic Press, New York, 1998).
[8] V. F. Nesterenko, *Dynamics of Heterogeneous Materials* (Springer, New York, 2011).
[9] G. Gallavotti, *The Fermi-Pasta-Ulam Problem: A Status Report* (Springer, Berlin, 2007).
[10] Y. Z. Wang, F. M. Li, and Y. S. Wang, Int. J. Mech. Sci. **106**, 357 (2016).
[11] W. J. Zhou, X. P. Li, Y. S. Wang, W. Q. Chen, and G. L. Huang, J. Sound Vib. **413**, 250 (2018).
[12] Y. Z. Wang and Y. S. Wang, Wave Motion **78**, 1 (2018).
[13] F. Li, P. Anzel, J. Yang, P. G. Kevrekidis, and C. Daraio, Nat. Commun. **5**, 5311 (2014).
[14] M. M. Sigalas and E. N. Economou, J. Sound Vib. **158**, 377 (1992).
[15] M. S. Kushwaha, Int. J. Mod. Phys. B **10**, 977 (1996).
[16] J. Cha and C. Daraio, Nature Nanotechnology **13**, 1016 (2018).
[17] X. Fang, J. Wen, B. Bonello, J. Yin, and D. Yu, Nat. Commun. **8**, 1288 (2017).
[18] C. Chong, E. Kim, E. G. Charalampidis, H. Kim, F. Li, P. G. Kevrekidis, J. Lydon, C. Daraio, and J. Yang, Phys. Rev. E **93**, 052203 (2016).
[19] W. H. Lin and C. Daraio, Phys. Rev. E **94**, 052907 (2016).
[20] C. Chong, M. A. Porter, P. G. Kevrekidis, and C. Daraio, J. Phys.: Condensed Matter **29**, 413003 (2017).
[21] W. Chen and D. L. Mills, Phys. Rev. Lett. **58**, 160 (1987).
[22] C. Conti, S. Trillo, and G. Assanto, Phys. Rev. E **57**, R1251 (1998).
[23] Y. S. Kivshar and N. Flytzanis, Phys. Rev. A **46**, 7972 (1992).
[24] N. Boechler, G. Theocharis, S. Job, P. G. Kevrekidis, M. A. Porter, and C. Daraio, Phys. Rev. Lett. **104**, 244302 (2010).
[25] M. Molerón, C. Chong, A. J. Martónez, M. A. Porter, P. G. Kevrekidis, and C. Daraio, New J. Phys. (2019), doi:10.1088/1367-2630/ab0118.
[26] L. N. Lupichev, A. V. Savin, and V. N. Kadantsev, *Synergetics of Molecular Systems* (Springer, Switzerland, 2015).
[27] M. Porter, P. Kevrekidis, and C. Daraio, Phys. Today **68**(11), 44 (2015).
[28] A. Spadoni and C. Daraio, Proc. Natl. Acad. Sci. USA **107**, 7230 (2010).
[29] H. A. Burgoyne, J. A. Newman, W. C. Jackson, and C. Daraio, Procedia Engineer. **103**, 52 (2015).
[30] M. Kurosu, D. Hatanaka, K. Onomitsu, and H. Yamaguchi, Nat. Commun. **9**, 1331 (2018).
[31] T. Singhal, E. Kim, T. Y. Kim, and J. Yang, Smart Mater. Struct. **26**, 055011 (2017).
[32] A. Scott, *Encyclopedia of Nonlinear Science* (Taylor and Francis, New York, 2006).
[33] P. J. Digby, J. Appl. Mech **48**, 803 (1981).
[34] S. Sen, M. Manciu, and J. D. Wright, Phys. Rev. E **57**, 2386 (1998).
[35] R. S. Sinkovits and S. Sen, Phys. Rev. Lett. **74**, 2686 (1995).
[36] E. Kim, F. Restuccia, J. Yang, and C. Daraio, Smart Mater. Struct. **24**, 125004 (2015).
[37] J. Lydon, G. Theocharis, and C. Daraio, Phys. Rev. E **91**, 023208 (2015).
[38] G. Theocharis, N. Boechler, and C. Daraio, *Nonlinear Periodic Phononic Structures and Granular Crystals* (Springer, Berlin/Heidelberg, 2013).
[39] L. Bonanomi, G. Theocharis, and C. Daraio, Phys. Rev. E **91**, 033208 (2015).
[40] H. M. Jaeger and S. R. Nagel, Science **255**, 1523 (1992).
[41] C. H. Liu and S. R. Nagel, Phys. Rev. Lett. **68**, 2301 (1992).
[42] A. C. Fischer-Cripps, *Contact Mechanics* (Springer, New York, 2011).
[43] M. A. Porter, C. Daraio, E. B. Herbold, I. Szelengowicz, and P. G. Kevrekidis, Physica D **238**, 666 (2009).
[44] S. Sen, J. Hong, J. Bang, E. Avalos, and R. Doney, Phys. Rep **462**, 21 (2008).
[45] R. Doney and S. Sen, Phys. Rev. Lett. **97**, 155502 (2006).
[46] C. Chong, F. Li, J. Yang, M. O. Williams, I. G. Kevrekidis, P. G. Kevrekidis, and C. Daraio, Phys. Rev. E **89**, 032924 (2014).
[47] E. Kim, F. Li, C. Chong, G. Theocharis, J. Yang, and P. G. Kevrekidis, Phys. Rev. Lett. **114**, 118002 (2015).
[48] F. S. Manciu and S. Sen, Phys. Rev. E **66**, 016616 (2002).
[49] C. Daraio, V. F. Nesterenko, E. B. Herbold, and S. Jin, Phys. Rev. Lett. **96**, 058002 (2006).
[50] G. Theocharis, N. Boechler, P. G. Kevrekidis, S. Job, M. A. Porter, and C. Daraio, Phys. Rev. E **82**, 056604 (2010).
[51] D. Khatri, C. Daraio, and P. Rizzo, Proc. SPIE **6934**, 69340U (2008).
[52] B. Liang, B. Yuan, and J. C. Cheng, Phys. Rev. Lett. **103**, 104301 (2009).
[53] N. Boechler, G. Theocharis, and C. Daraio, Nat. Mater. **10**, 665 (2011).
[54] C. Daraio, V. F. Nesterenko, E. B. Herbold, and S. Jin, Phys. Rev. E **72**, 016603 (2005).
[55] V. F. Nesterenko, C. Daraio, E. B. Herbold, and S. Jin, Phys. Rev. Lett. **95**, 158702 (2005).
[56] J. Cuevas-Maraver, P. G. Kevrekidis, A. Vainchtein, and H. Xu, Phys. Rev. E **96**, 032214 (2017).
[57] V. F. Nesterenko, Prikl. Mekh. Tekh. Fiz. **24**, 136 (1983) [J. Appl. Mech. Phys. **24**, 733 (1983)].
[58] G. James and D. Pelinovsky, Proc. R. Soc. A **470**, 20130462 (2014).
[59] Y. Shen, P. G. Kevrekidis, S. Sen, and A. Hoffman, Phys. Rev. E **90**, 022905 (2014).
[60] M. L. Wang, Phys. Lett. A **199**, 169 (1995).
[61] M. L. Wang, Phys. Lett. A **213**, 279 (1996).
[62] M. L. Wang, Y. Zhou, and Z. B. Li, Phys. Lett. A **216**, 67 (1996).
[63] J. L. Zhang, Z. G. Liu, S. W. Li, and M. L. Wang, Phys. Scripta **86**, 015401 (2012).
[64] J. L. Zhang and Z. G. Liu, Commun. Theor. Phys. **56**, 1111 (2011).
[65] J. Hietarinta, Phys. Rev. Lett. **27**, 1192 (1971).
[66] A. D. Martin, C. S. Adams, and S. A. Gardiner, Phys. Rev. Lett. **98**, 020402 (2007).

[67] R. Seydel, *Practical Bifurcation and Stability Analysis* (Springer Verlag, New York, 2010).
[68] L. Ta-Tsien, Z. Yi, and K. De-Xing, Nonlin. Anal. **28**, 1299 (1997).
[69] G. Couton, H. Maillotte, and M. Chauvet, J. Opt. B: Quant. Semiclass. Opt. **6**, S223 (2004).
[70] Z. Chen, M. Segev, S. R. Singh, T. H. Coskun, and D. N. Christodoulides, J. Opt. Soc. Am. B **14**, 1407 (1997).
[71] G. P. Agrawal, *Nonlinear Fiber Optics* (Academic, New York, 1995).
[72] S. Trillo and W. Torruellas, *Spatial Solitons*, Vol. 82, 1st ed. (Springer, Berlin, 2001).
[73] P. G. Kevrekidis, *The Discrete Nonlinear Schrödinger Equation* (Springer, Berlin/Heidelberg, 2009).
[74] N. Akhmediev, A. Ankiewicz, and M. Taki, Phys. Lett. A **373**, 675 (2009).
[75] A. Chabchoub, N. P. Hoffmann, and N. Akhmediev, Phys. Rev. Lett. **106**, 204502 (2011).
[76] E. G. Charalampidis, J. Lee, P. G. Kevrekidis, and C. Chong, Phys. Rev. E **98**, 032903 (2018).
[77] I. Nikolkina and I. Didenkulova, Nat. Hazards: Earth Syst. Sci. **11**, 2913 (2011).
[78] E. M. Bitner-Gregersen and A. Toffoli, Ocean Dynam. **64**, 1457 (2014).
[79] P. J. Olver, *Application of Lie Groups to Differential Equation*, 2nd ed. (Springer, New York, 1993).
[80] D. Khatri, D. Ngo, and C. Daraio, Granular Matter **14**, 63 (2012).